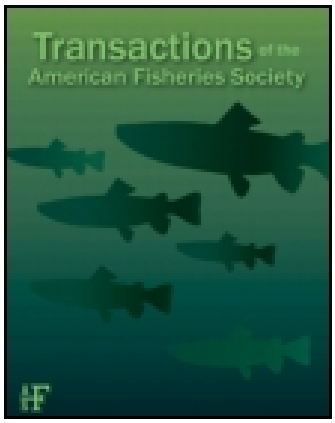

Transactions of the American Fisheries Society
Publication details, including instructions for authors and subscription information:
http://www.tandfonline.com/loi/utaf20

Individual-Based Modeling of Delta Smelt Population Dynamics in the Upper San Francisco Estuary: I. Model Description and Baseline Results

Kenneth A. Rose [a], Wim J. Kimmerer [b], Karen P. Edwards [c] & William A. Bennett [d]

[a] Department of Oceanography and Coastal Sciences, Louisiana State University, Energy, Coast, and Environment Building, Baton Rouge, Louisiana, 70803, USA

[b] Romberg Tiburon Center for Environmental Studies, San Francisco State University, 3152 Paradise Drive, Tiburon, California, 94920, USA

[c] Environment Agency, Manley House, Kestrel Way, Exeter, EX2 7LQ, UK

[d] Center for Watershed Sciences, John Muir Institute of the Environment, Bodega Marine Laboratory, University of California, Davis, Post Office Box 247, Bodega Bay, California, 94923, USA

Published online: 01 Aug 2013.

To cite this article: Kenneth A. Rose, Wim J. Kimmerer, Karen P. Edwards & William A. Bennett (2013) Individual-Based Modeling of Delta Smelt Population Dynamics in the Upper San Francisco Estuary: I. Model Description and Baseline Results, Transactions of the American Fisheries Society, 142:5, 1238-1259, DOI: 10.1080/00028487.2013.799518

To link to this article: http://dx.doi.org/10.1080/00028487.2013.799518

Transactions of the American Fisheries Society 142:1238–1259, 2013

ISSN: 0002-8487 print / 1548-8659 online
DOI: 10.1080/00028487.2013.799518

ARTICLE

Individual-Based Modeling of Delta Smelt Population Dynamics in the Upper San Francisco Estuary: I. Model Description and Baseline Results

Kenneth A. Rose*
Department of Oceanography and Coastal Sciences, Louisiana State University, Energy, Coast, and Environment Building, Baton Rouge, Louisiana 70803, USA

Wim J. Kimmerer
Romberg Tiburon Center for Environmental Studies, San Francisco State University, 3152 Paradise Drive, Tiburon, California 94920, USA

Karen P. Edwards
Environment Agency, Manley House, Kestrel Way, Exeter EX2 7LQ, UK

William A. Bennett
Center for Watershed Sciences, John Muir Institute of the Environment, Bodega Marine Laboratory, University of California, Davis, Post Office Box 247, Bodega Bay, California 94923, USA

Abstract

Many factors have been implicated in the decline of Delta Smelt *Hypomesus transpacificus* in the upper San Francisco Estuary, and the importance of each factor is difficult to determine using field data alone. We describe a spatially explicit, individual-based population model of Delta Smelt configured for the upper estuary. The model followed the reproduction, growth, mortality, and movement of individuals over their entire life cycle on the same spatial grid of cells as the Delta Simulation Model (DSM2) hydrodynamics model. Daily values of water temperature, salinity, and densities of six zooplankton prey types were represented on the spatial grid. Reproduction was evaluated daily, and new individuals were introduced into the model as yolk sac larvae. Growth of feeding individuals was based on bioenergetics and zooplankton densities. Mortality sources included natural mortality, starvation, and entrainment in water diversion facilities. Movement of larvae was determined using a particle tracking model, while movement of juveniles and adults was based on salinity. Simulations were performed for 1995–2005. The baseline simulation was generally consistent with the available data. Predicted daily fractions of larvae entrained and annual fractions of adults entrained were similar in magnitude to data-based estimates but showed less interannual variation. Interannual differences in mean length at age 1 had large effects on maturity and subsequent egg production. Predicted and observed spatial distributions in the fall showed moderately good agreement for extremely low- and high-outflow years. As indicated by the population growth rate, 1998 was the best year and 2001 was the worst year. Water year 1998 (i.e., October 1997–September 1998) was characterized by fast growth in fall 1997, low entrainment, and high stage-specific survival rates, whereas water year 2001 had opposite conditions. Our analysis further shows how multiple factors can operate simultaneously to result in the decline in abundance of Delta Smelt.

*Corresponding author: karose@lsu.edu
Received November 9, 2012; accepted April 18, 2013
Published online August 1, 2013

Understanding the critical drivers and environmental changes that influence the population dynamics of fish is vital for effective resource management and restoration. Most fish species live multiple years and show ontogenetic shifts in the habitats they utilize, which exposes them to multiple environmental and biological factors spread over several points in their life cycle (Rose 2000). Identification of the relative importance of these factors and how they may interact with each other is an important step toward understanding and managing fish populations. A major debate is underway about the status of many harvested marine and coastal fish populations (Myers and Worm 2003; Hilborn 2007; Worm et al. 2009), as human development of coastal areas (McGranahan et al. 2007) and demand for high-quality freshwater (Vörösmarty et al. 2000) continue to accelerate. Identification of the major factors affecting population dynamics (especially declines in population) is critical because the high economic costs of protection and restoration demand efficient and effective responses.

The need to understand mechanisms of population decline for Delta Smelt *Hypomesus transpacificus* in the San Francisco Estuary is critical. This endemic species is listed as threatened under the U.S. Endangered Species Act and is listed as endangered under the California Endangered Species Act. Delta Smelt have generally been at low abundance since the 1980s and showed an even further sharp decrease starting in about 2002 (Bennett 2005; Sommer et al. 2007; Thomson et al. 2010). Delta Smelt have also become the focus of contentious debate because of perceived conflicts between the conservation of this species and the operation of facilities that divert water from the Delta Smelt's habitat for agricultural and urban uses (Brown et al. 2009; NRC 2010). These facilities alter seasonal patterns of flow, and they entrain and kill large numbers of Delta Smelt (Kimmerer 2008).

Many factors may be involved in the decline of Delta Smelt, and quantifying the importance of each factor has proven to be elusive despite the availability of extensive long-term field data (NRC 2012). Factors examined as possible contributors to the decline include entrainment of Delta Smelt by the two large water diversion facilities in the Sacramento–San Joaquin River Delta (hereafter, "the Delta"), shifts in the composition and densities of the zooplankton (prey) community, and changes in physical habitat related to salinity and turbidity (Baxter et al. 2010). A sharp decline in four fish species (juvenile Striped Bass *Morone saxatilis*; Longfin Smelt *Spirinchus thaleichthys*; Threadfin Shad *Dorosoma petenense*; and Delta Smelt) within the upper San Francisco Estuary beginning in approximately 2000 led to a substantial effort at synthesizing existing data to determine the cause (Sommer et al. 2007). The results to date have narrowed the possible factors to some extent (e.g., contaminant effects are likely small) and have facilitated the conclusion that the recent decline in Delta Smelt was due to multiple factors acting together (Baxter et al. 2010). Two statistical analyses (Mac Nally et al. 2010; Thomson et al. 2010) examined the dynamics of the four fish species by using monitoring data collected from the 1970s to 2007. Both analyses, which used similar data but different statistical methods, showed several covariates that were related to abundance of the fish, but they could not resolve the cause of the recent declines.

An alternative approach to the analysis of the effects of multiple factors on fish populations is simulation modeling of the growth, mortality, reproduction, and movement processes underlying the population dynamics. Population modeling allows the investigator to control everything and thus to perform simulation experiments for isolating the effects of individual factors and for exploring the effects of previously unobserved combinations of conditions (Rose et al. 2009). However, model results must be interpreted with caution because models are always simplifications of reality, and their predictions can be biased by decisions about which processes to include and at what temporal and spatial scales to represent those processes.

In this paper, we describe a spatially explicit, individual-based population model of Delta Smelt configured for the upper San Francisco Estuary. We chose this approach because many of the factors that are thought to contribute to the Delta Smelt's decline vary in space (Baxter et al. 2010), and simulating fish movement is more straightforward with an individual-based approach than with other modeling approaches (Tyler and Rose 1994). We first briefly describe the San Francisco Estuary and the life cycle of Delta Smelt. We then describe the spatial grid, environmental conditions, and reproduction, growth, mortality, and movement processes that are represented in the individual-based model. Hydrodynamic model output for the spatial grid and field data for temperature, salinity, and zooplankton densities were used as inputs to the population model for simulation of the period 1995–2005. The results of the baseline simulation are compared with the observed data, and we contrast the conditions between a "good year" and a "bad year" for Delta Smelt growth and survival within the baseline simulation. We conclude with a discussion of our results relative to other analyses and the strengths and weaknesses of our current model formulation. In our companion paper (Rose et al. 2013, this issue), we show that the results presented here are robust to alternative baseline assumptions, and we further explore the factors causing good and bad years by using a simulation experiment approach.

UPPER SAN FRANCISCO ESTUARY AND DELTA SMELT

The San Francisco Estuary is the largest estuary on the U.S. Pacific coast, with a watershed covering approximately 40% of California (Figure 1). The estuary connects the Sacramento and San Joaquin rivers through San Francisco Bay to the Pacific Ocean. Freshwater enters via the Sacramento River from the north and the San Joaquin River from the south; the confluence is roughly the landward limit of ocean salt penetration (Kimmerer 2004). We focus on the upper portion of the estuary (including the Delta and Suisun Bay), which encompasses the entire range of the Delta Smelt.

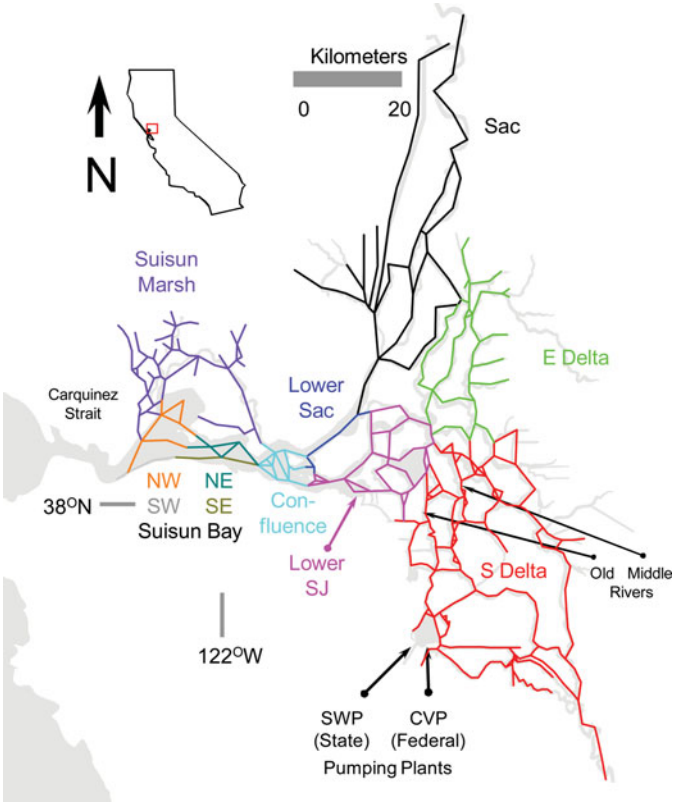

FIGURE 1. Location of the San Francisco Estuary, California, and the spatial grid and boxes used in the model. Gray represents the outline of the estuary. The 11 boxes are color coded and refer to (in numerical order): (1) Sacramento River region (Sac) of the Sacramento–San Joaquin Delta; (2) eastern Delta (E Delta); (3) southern Delta (S Delta); (4) lower Sacramento River region (Lower Sac); (5) lower San Joaquin River region (Lower SJ); (6) confluence (westernmost box in the Delta); (7) southeast Suisun Bay (SE); (8) northeast Suisun Bay (NE); (9) Suisun Marsh; (10) southwest Suisun Bay (SW); and (11) northwest Suisun Bay (NW). Additional labels show the Old River, Middle River, Carquinez Strait, and the State Water Project (SWP) and Central Valley Project (CVP) pumping plants.

The San Francisco Estuary has been described as one of the most highly altered estuarine ecosystems in the world (Nichols et al. 1986; Lund et al. 2010). Over the past 150 years, approximately 95% of the marshes surrounding the estuary have been isolated from tidal action, and numerous nonnative species have been introduced—some with substantial ecological effects (e.g., Nichols et al. 1990; Winder and Jassby 2011). The Delta, which formerly consisted of tidal marsh, is now a complex network of linked channels and sloughs surrounding islands that are protected by a constructed levee system. During the past 60 years, the upper estuary has increasingly been managed through large-scale manipulation of river flows in order to provide freshwater for agricultural, municipal, and industrial uses.

The two large water diversions in the south Delta have exported an average of 30% of the available flow into the Delta during 1960–2000, with the percentage generally increasing through time and exceeding 60% in some years and seasons (Kimmerer 2004). The State Water Project (SWP) facility provides drinking water for over 23 million Californians, and together the two diversion facilities (the SWP and the Central Valley Project [CVP]) fuel an estimated $\$25 \times 10^9$ annual agricultural economy (Grimaldo et al. 2009). Elaborate fish recovery facilities attempt to screen fish from the diverted water but with mixed success (Kimmerer 2011). All of these changes have substantially altered both the physical and ecological aspects of the system (Nichols et al. 1986; Hollibaugh 1996; NRC 2012).

The life history of the Delta Smelt is summarized briefly here based on several sources (Moyle et al. 1992; Moyle 2002; Bennett 2005). The Delta Smelt has a relatively unusual life history strategy (Bennett 2005), as it exhibits the small size and short life span that are typical of an opportunistic life history strategy, but it has low reproductive rates that are more similar to those of an equilibrium strategist (Winemiller and Rose 1992). The Delta Smelt's life history also somewhat resembles those of salmonids (McCann and Shuter 1997) but without parental care. The geographic range of the Delta Smelt is confined to the upper San Francisco Estuary. It is primarily an annual species but with some small fraction of the population surviving a second year to spawn. Spawning takes place in freshwater during February–May at temperatures between 12°C and 20°C; spawning appears to be clustered in 2-week intervals, presumably related to the spring–neap tidal cycle. Eggs are demersal and attached; larval stages generally rear in freshwater before being transported to brackish waters, which are typically located between the confluence of the San Joaquin and Sacramento rivers and Carquinez Strait at the seaward margin of Suisun Bay (Figure 1). All life stages remain at a salinity of about 0.5–6.0 psu (the low-salinity zone) until the end of the year, when migration to freshwater begins. Delta Smelt eat primarily zooplankton throughout their lives, although adults also eat epibenthic crustaceans, such as amphipods. Delta Smelt are consumed by a variety of fish, principally visual predators.

MODEL DESCRIPTION

Overview

The model followed the reproduction, growth, mortality, and movement of individual Delta Smelt over their entire life cycle on a spatial grid of cells (Figure 1). The spatial grid was a one-dimensional network of 517 channels and 5 reservoirs used in the Delta Simulation Model (DSM2) hydrodynamic model (California Department of Water Resources [CDWR]). This one-dimensional model simulates non-steady-state hydrodynamics in a network of channels and has been widely used for analyses and water supply planning for the Delta (Kimmerer and Nobriga 2008). Simulations from DSM2 provided (1) hourly water velocities and water levels at the ends of channels and (2) hourly water flows into and out of the reservoirs. Daily water temperature, salinity, and densities of six zooplankton prey types as estimated from field data were also represented on the same spatial grid.

Each 365-d model year began on October 1, the start date for each water year. Individuals were aged on January 1 of each year. Whenever we refer to a year, it is the year that includes the summer period (e.g., model year 1996 extended from October 1, 1995, to September 30, 1996). Multiyear simulations were performed using reproduction to introduce the new individuals each year.

Reproduction was evaluated daily during the spring spawning season, and eggs developed as a daily cohort at a temperature-dependent rate. Upon hatching, new yolk sac larvae were pooled for each day and were introduced as model individuals. Individuals developed through life stages of yolk sac larva, larva, postlarva, juvenile, and adult. Growth was based on bioenergetics and zooplankton densities in the grid cells. Mortality included a stage-specific mortality rate, starvation, and mortality due to entrainment at the water diversion facilities. Movement of yolk sac larvae, larvae, and postlarvae was determined hourly by using a particle tracking model (PTM) that incorporates water velocities from the DSM2 hydrodynamic model. Movement of juveniles and adults was based entirely on a behavioral response to salinity, and the locations of individual fish on the grid were updated every 12 h.

All simulations used hydrodynamic conditions, temperature, salinity, and zooplankton densities for the period 1995–2005. This period was selected because (1) it encompasses the main period of Delta Smelt decline, (2) hydrodynamic simulations were available, and (3) field data on zooplankton and Delta Smelt were relatively complete.

Environment

A second grid of 11 coarser boxes was overlaid onto the channel grid (Figure 1) so that the more sparsely sampled field data could be used to specify daily water temperature, salinity, and zooplankton densities. The 11 boxes were determined based on previously identified regions of hydraulic similarity (e.g., Miller et al. 2012) and the availability of enough stations to ensure that at least several stations were present in each box.

Daily values of temperature, salinity, and zooplankton densities were estimated for each box and then were assigned to each channel within each box on each day (see details in Supplement A in the online version of this article). Final daily temperature and salinity values for each box are shown in Figure 2 for a year with high freshwater outflow (1998) and a year with low freshwater outflow (2001). All channels within a given box were assigned the box values. Temperature did not vary much among sampling stations within boxes, and the sampling density was too low to represent the within-box (channel-level) spatial gradients in salinity.

The food environment was represented by the biomasses of six zooplankton types: adults of *Limnoithona* spp. (calanoid copepods), calanoid copepodids, other calanoid adults, adult *Eurytemora* (calanoid copepods), adult *Acanthocyclops vernalis* (cyclopoid copepods), and adult *Pseudodiaptomus* (calanoid copepods). We included random variation when we used the boxwide mean to assign values to the channels within each box (see Supplement A). Daily zooplankton biomass densities in each box are presented for the same high-outflow (Figure 3) and low-outflow (Figure 4) years as were shown for temperature and salinity.

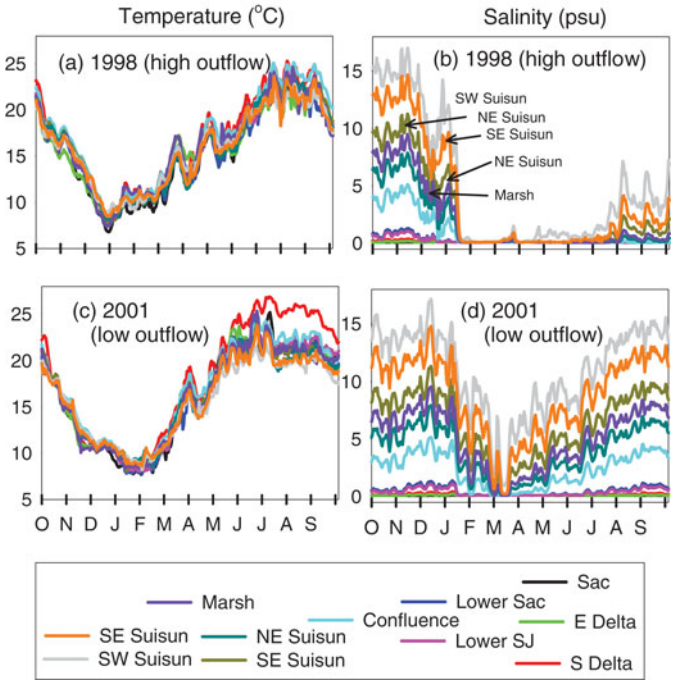

FIGURE 2. Daily temperature and salinity values in each box for **(a)**, **(b)** 1998 (a year of high outflow) and **(c)**, **(d)** 2001 (a year of low outflow). See Figure 1 for definition of box abbreviations. [Figure available online in color.]

Spawning

Each female individual that was longer than 60 mm TL at the start of the spawning season was allowed to spawn up to two times within the spawning season. We used a simple threshold of 60 mm because it was well supported by data (Bennett 2005) and because the manner in which maturity varies around the 60-mm length was uncertain. We explore a smoother maturity function in our companion paper (Rose et al. 2013).

The earliest day of spawning was first determined each year on October 1 by looking ahead at temperatures and finding the first day on which temperature exceeded 12°C in any box. On the earliest possible day of spawning in each year, a temperature of first actual spawning was assigned to each mature individual from a uniform distribution between 12°C and 20°C. To mimic the clustering of spawning on spring–neap tidal cycles, an individual spawned at the end of the 14-d tidal cycle that followed the day when water temperature in that individual's channel exceeded its assigned spawning temperature. By the time of spawning, the migratory movement algorithm based on salinity had put adults near or into freshwater boxes.

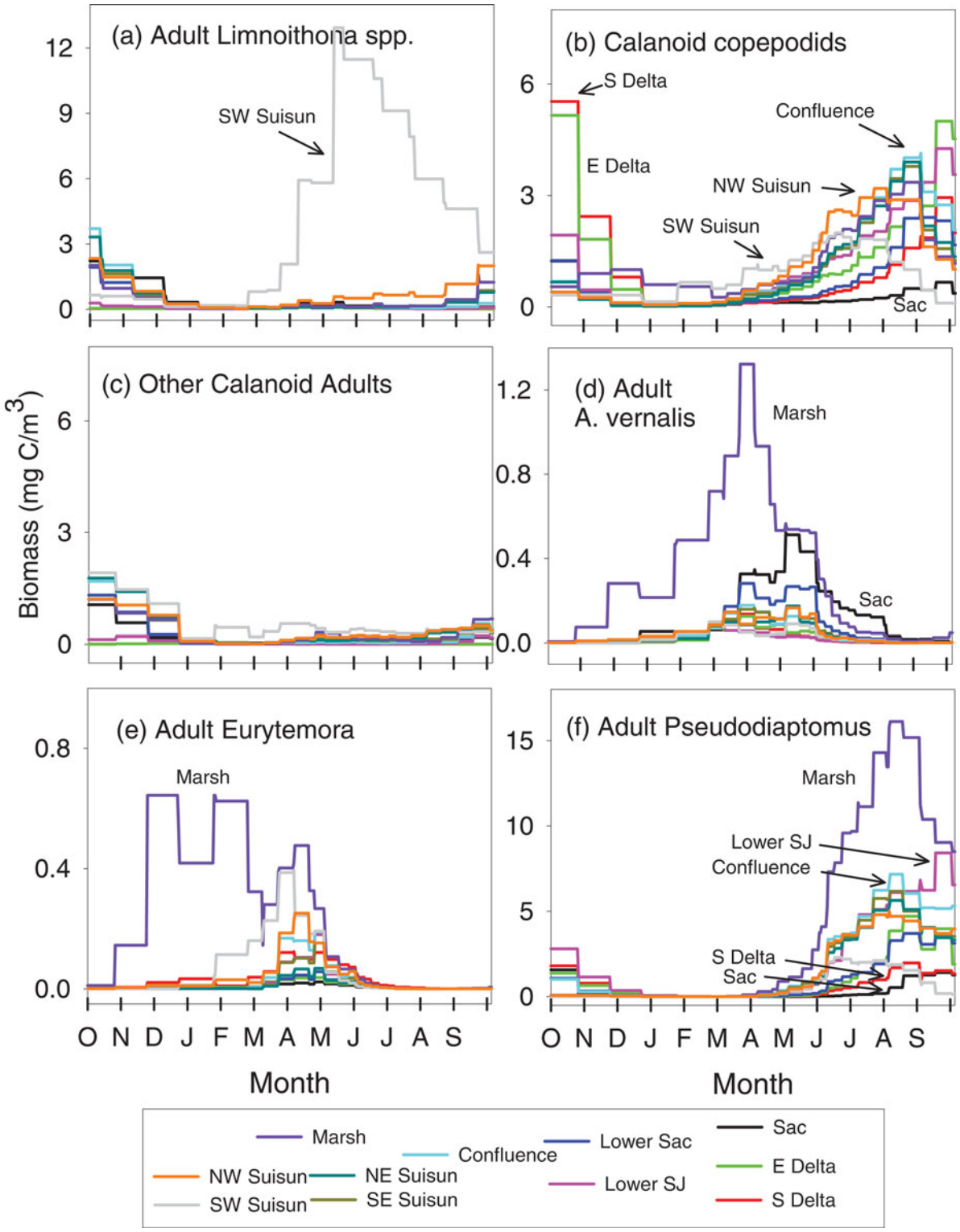

FIGURE 3. Daily biomass density values (mg C per m^3 of water) for each of the six zooplankton groups in each spatial box during a year of high outflow (1998): **(a)** adults of *Limnoithona* spp., **(b)** calanoid copepodids, **(c)** other calanoid adults, **(d)** adult *Acanthocyclops vernalis*, **(e)** adult *Eurytemora*, and **(f)** adult *Pseudodiaptomus*. See Figure 1 for definition of box abbreviations. [Figure available online in color.]

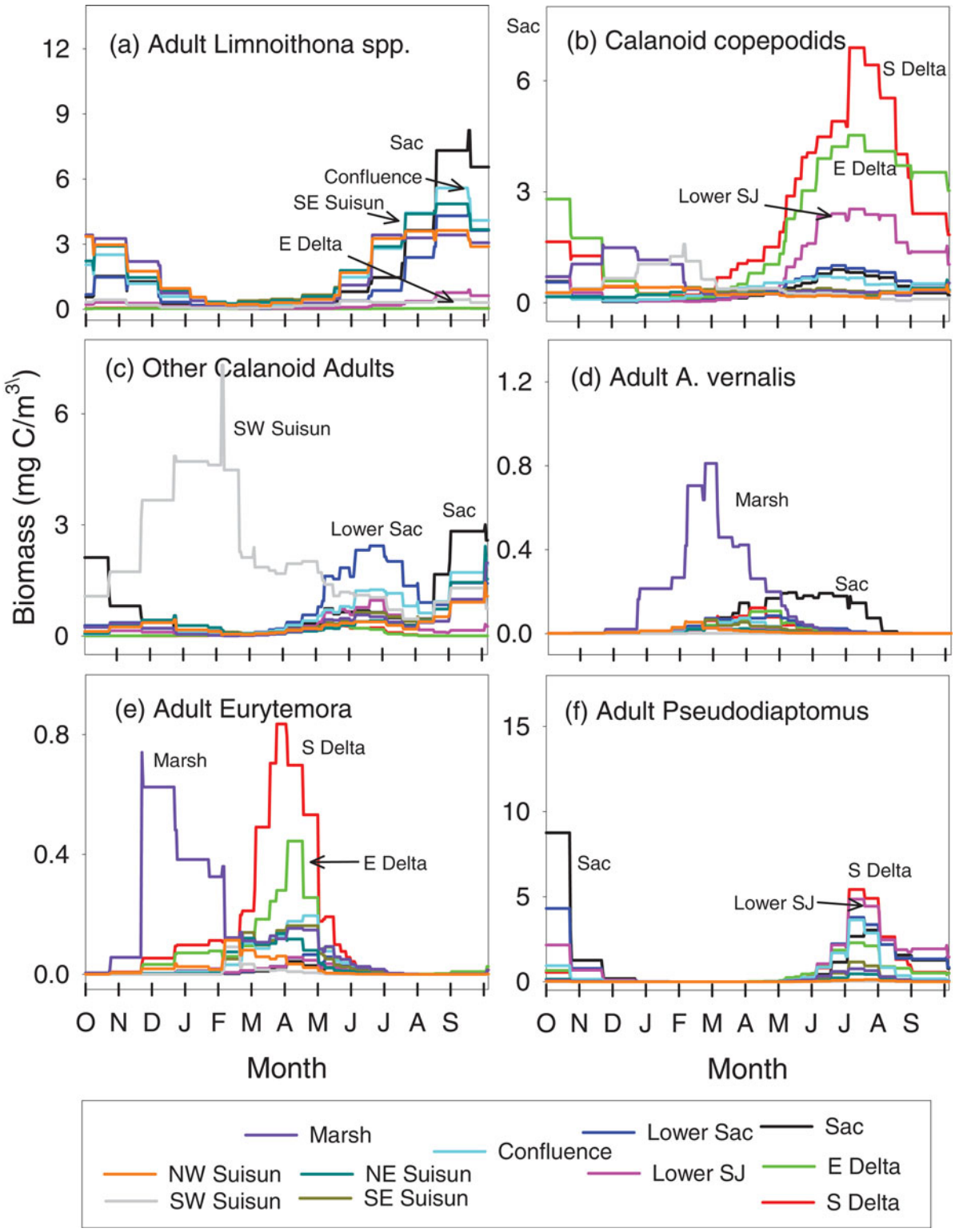

FIGURE 4. Daily biomass density values (mg C per m^3 of water) for each of the six zooplankton groups in each spatial box during a year of low outflow (2001): **(a)** adults of *Limnoithona* spp., **(b)** calanoid copepodids, **(c)** other calanoid adults, **(d)** adult *Acanthocyclops vernalis*, **(e)** adult *Eurytemora*, and **(f)** adult *Pseudodiaptomus*. See Figure 1 for definition of box abbreviations. [Figure available online in color.]

Fecundity (D; eggs/female) depended on the individual's weight on the day of spawning (Bennett 2005),

$$D = 175.4e^{\frac{L_{equiv}}{28.3}}, \quad (1)$$

where L_{equiv} (mm) is the length based on the actual weight of the fish. Upon spawning, the body weight of the individual Delta Smelt was reduced by 15%. We treated males the same as females (i.e., spawning temperatures and weight loss), but without any contribution of eggs, to produce similar weights at age.

After their first spawning event, females were evaluated daily to determine whether they would spawn a second time. Second spawning occurred if (1) the individual had regained enough weight (>95% of the weight expected from its length), (2) 14 or more days had passed since the first spawning, and (3) it was not too late (too warm) in the season for that individual to spawn in its box. The last possible day of spawning in each box was calculated as the first day after temperature exceeded 20°C plus 14 d to allow for the final tidal cycle to complete. The fecundity relationship used for the second spawning was the same as that for the first spawning, and weight was again reduced by 15%.

Eggs

Each female's first and second (if it occurred) spawns of eggs were followed separately as cohorts until hatching, when they became yolk sac larvae. Day of hatching was determined for each cohort by accumulating the daily fractional egg development (DV_e) until the degree of development exceeded 1.0. The daily fractional development towards hatching was based on temperature (Bennett 2005),

$$DV_e = \frac{1}{28.1 - 1.1 \cdot T}, \quad (2)$$

where T is the daily temperature (°C) in the box where spawning occurred. Spawning box temperature (which varied daily) was used because the eggs are attached. All eggs in each cohort that was spawned in a given box on a given day hatched on the same day. Daily egg mortality rates (M; d^{-1}) were calculated by converting hatch rates observed at constant temperature in the hatchery to daily mortality (Bennett 2005),

$$M = \frac{-\log(s)}{DV_e} \quad (3)$$

and

$$s = -2.35 + 0.45 \cdot T - 0.016 \cdot T^2, \quad (4)$$

where s is the survival fraction through the egg stage.

Yolk Sac Larvae

Beginning with yolk sac larvae, new model individuals were created and followed for the rest of their lives. New individuals were created from all those that hatched in each box on each day, and they were distinguished by whether they came from a first or second spawning event. Length (L; mm) at hatch depended on the temperature on the day of hatching (Bennett 2005),

$$L = 5.92 - 0.05 \cdot T. \quad (5)$$

Weight (g wet weight) at hatch was determined from a field-based length–weight relationship (Kimmerer et al. 2005):

$$W = 0.005 \cdot L^3. \quad (6)$$

Similar to the method used for eggs, the duration of the yolk sac larval stage was determined by accumulating the daily fractional development (DV_y) of each model individual based on the temperature in its box (Bennett 2005) until the cumulative development exceeded 1.0:

$$DV_y = \frac{1}{7.53 - 0.08 \cdot T}. \quad (7)$$

Daily mortality rate of yolk sac larvae was assumed constant (0.035 d^{-1}) and was a key parameter adjusted as part of model calibration.

Feeding Life Stages: Development and Bioenergetics

Larvae became postlarvae at 15 mm, and postlarvae became juveniles at 25 mm; juveniles then became age-1 adults and age-1 adults from the previous year advanced to age 2 on January 1 (Bennett 2005). Age-2 adults were removed from the model just before attaining age 3. Larval to postlarval development coincided with the development of a swim bladder, and the juvenile stage marked the appearance of fin folds and an association with the low-salinity zone.

The daily growth of each feeding individual was represented by a difference form of the Wisconsin bioenergetics model (Ney 1993; Hanson et al. 1997),

$$W_t = W_{t-1} + (C - R - F - U - SDA) \cdot W_{t-1} \cdot \frac{e_p}{e_s} - Sp \cdot W_{t-1}, \quad (8)$$

where W is the weight of each individual, C is the realized consumption rate, R is the total metabolic rate, F is egestion, U is excretion, SDA is specific dynamic action, and Sp is loss due to spawning. All rates except Sp were in units of grams of prey per gram of Delta Smelt per day (g prey·g $smelt^{-1}$·d^{-1} in wet weight); Sp was the fraction of weight lost (0.15) and occurred only on the day of spawning. The e_p and e_s terms (J/g) were used to convert grams of prey per gram of Delta Smelt to grams of smelt per gram of smelt, which was then multiplied by weight (W) to yield the weight change in grams of Delta Smelt per individual per day. The value of e_s was fixed at 4,814 J/g, while e_p was computed each day based on the fraction of *Limnoithona* in

the diet. All zooplankton groups had an energy density of 2,590 J/g; the exception was *Limnoithona*, for which energy density was assumed to be 30% lower (1,823 J/g) because Delta Smelt grow more slowly when fed *Limnoithona* (Lindsay Sullivan, San Francisco State University, personal communication).

Total length (L; mm) was obtained from weight by using equation (6). Length was partially uncoupled from weight because length was allowed only to increase, whereas fish could lose weight. On days of weight gain, length was increased only after the individual's weight equaled that expected from its length. Thus, fish were allowed to become skinny but not fat.

Maximum consumption (C_{max}) depended on an individual's weight (W) and the water temperature (T):

$$C_{max} = a_c W^{b_c} f(T). \tag{9}$$

The temperature adjustment to maximum consumption ($f[T]$) increased from a value of CK_1 at temperature CQ to 0.98 at temperature T_O and then stayed at 0.98 until temperature reached T_M, after which the adjustment declined to CK_4 as temperature approached T_L (Table 1).

Realized consumption by the ith fish (C_i) was a functional response that depended on C_{max} and the densities of each zooplankton group j (prey density, PD_j) in the same channel as the fish:

$$C_{ij} = \frac{C_{max} W_i \left(\frac{PD_j \cdot V_{ij}}{K_{ij}}\right)}{1 + \sum_{k=1}^{6} \left(\frac{PD_k \cdot V_k}{K_{ik}}\right)} \tag{10}$$

and

$$C_i = \sum_{j=1}^{6} C_{ij}, \tag{11}$$

where C_{ij} is the daily rate of consumption of the jth prey type (six zooplankton groups) by individual fish i; V_{ij} is the vulnerability of prey type j to fish i; and K_{ik} is the half-saturation constant for fish i feeding on each prey type k. Equations (10) and (11) allowed an individual fish to consume multiple prey types without exceeding its maximum consumption. Vulnerabilities (V_{ij}) were set to 1.0 for all life stages eating all zooplankton types; the exception was Delta Smelt larvae, for which V_{ij} values of zero were used for all adult prey groups other than *Limnoithona* spp. The K-values were calibrated outside of the model to obtain diet and consumption rates that appeared realistic (Supplement B in the online version of this article).

The total metabolic rate (R) was an allometric function of weight and used an exponential relationship ($g[T]$) to adjust metabolism for temperature:

$$R = a_r W^{b_r} \cdot g(T), \tag{12}$$

where

$$g(T) = e^{(R_Q \cdot T)}. \tag{13}$$

Egestion (F) was a constant fraction of consumption, while *SDA* and excretion (U) were fractions of net assimilated energy

TABLE 1. Parameter values for each Delta Smelt life stage in the bioenergetics model.

Parameter	Description	Larvae	Postlarvae	Juveniles and adults
	Maximum consumption (C_{max})			
a_c	Weight multiplier	0.18	0.18	0.1
b_c	Weight exponent	−0.275	−0.275	−0.54
CQ (°C)	Temperature at CK_1 of maximum	7	10	10
T_O (°C)	Temperature at 0.98 of maximum	17	20	20
T_M (°C)	Temperature at 0.98 of maximum	20	23	23
T_L (°C)	Temperature at CK_4 of maximum	28	27	27
CK_1	Effect at temperature CQ	0.4	0.4	0.4
CK_4	Effect at temperature T_L	0.01	0.01	0.01
	Metabolism (R)			
a_r	Weight multiplier	0.0027	0.0027	0.0027
b_r	Weight exponent	−0.216	−0.216	−0.216
R_Q	Exponent for temperature effect	0.036	0.036	0.036
S_d	Fraction of assimilated food lost to *SDA*	0.175	0.175	0.175
	Egestion (F) and excretion (U)			
F_a	Fraction of consumed food lost to egestion	0.16	0.16	0.16
U_a	Fraction of assimilated food lost to excretion	0.1	0.1	0.1

($C - F$; Table 1):

$$F = F_a \cdot C, \tag{14}$$

$$SDA = S_d \cdot (C - F), \tag{15}$$

and

$$U = U_a \cdot (C - F). \tag{16}$$

During calibration, we adjusted the bioenergetics parameter values developed for Rainbow Smelt *Osmerus mordax* (Lantry and Stewart 1993) until we obtained growth that was realistic for Delta Smelt. We adjusted the allometric and temperature-related parameter values of maximum consumption (a_c, b_c, CQ, T_O, T_M, and T_L in Table 1) and the temperature parameter that affected respiration (R_Q in Table 1). We determined parameter values that satisfied two conditions: (1) realistic daily growth rates and optimal temperatures for growth for mid-stage-sized larvae, juveniles, and adults; and (2) realistic weights and lengths for an individual that had grown from first feeding through age 2 under daily average temperatures and a consumption rate (C) that was equal to 0.8 of the maximum (i.e., proportion of maximum consumption [p-value] = 0.8; $C = p$-value $\times$ C_{max}). The final bioenergetics rates for the mid-stage-sized larvae, postlarvae, juveniles, and adults are shown in Supplement B.

Mortality

Mortality occurred from stage-specific mortality rates (M), starvation, entrainment losses at the two water export pumping facilities, and old age. Stage-specific mortality rates represented predation and other causes of mortality not explicitly calculated from starvation or entrainment. Daily instantaneous mortality was temperature dependent for eggs (equations 3 and 4); M was set at 0.035 for yolk sac larvae (calibrated), 0.05 for larvae, 0.03 for postlarvae, 0.015 for juveniles, and 0.006 for adults. Starvation occurred if the weight of an individual fell below 50% of the weight expected from its length. Upon reaching age 3 (i.e., the individual's third January 1), the individual died from old age and was removed from the population.

Entrainment mortality for all life stages except eggs occurred when an individual entered Clifton Court Forebay (reservoir number 4; SWP) or arrived at node 181 (CVP; Figure 1). Yolk sac larvae, larvae, and postlarvae were transported there by the PTM, whereas juveniles and adults were unaffected by hydrodynamic conditions except through salinity. Use of only those individual juveniles and adults that arrived at the SWP and CVP by behavioral movements based on salinity resulted in underestimation of the numbers entrained by the pumping facilities. Delta Smelt are recovered at the south Delta fish facilities at higher rates when daily net flow in the southern Delta (Middle and Old rivers) is southwards toward the SWP and CVP (Grimaldo et al. 2009; Kimmerer 2011). Therefore, juveniles and adults that were located in the south Delta box (box 3) of the model were exposed to additional entrainment mortality of 0.02 d^{-1} whenever the daily averaged flow in Middle River (downstream end of channel 90; Figure 1) was southward. The value of the added mortality (0.02 d^{-1}) was determined as part of model calibration.

Movement

Yolk sac larvae, larvae, and postlarvae were transported by water velocities on the spatial grid hourly by using a particle tracking approach, whereas juveniles and adults were moved every 12 h by using a kinesis approach to behavioral movement.

The PTM was a recoded version of the CDWR's PTM and used the same formulations (Wilbur 2000; Miller 2002). The CDWR's PTM has been used to examine entrainment impacts (e.g., Kimmerer and Nobriga 2008) and has been compared with other PTMs (Gross et al. 2010). Our recoded version used as input the hourly values of velocity at each end of each channel and the water level at each node that was generated by the DSM2 hydrodynamic model. The PTM kept track of the hourly positions of particles (the three larval stages) in three dimensions: along-channel (x = distance [m] from the upstream end of a channel), lateral (y = distance [m] from the center line of the channel), and vertical (z = distance [m] from the bottom of the channel). The y and z positions within a channel were altered by random perturbations and were used to adjust the x-direction velocity (Supplement C in the online version of this article).

Day-to-day movements and seasonal migrations of juveniles and adults were based on a kinesis approach (Humston et al. 2000, 2004), with salinity used as the cue. Salinity was used to simulate reasonable distributions of individuals within the system, but salinity did not directly affect growth or mortality. Rather, salinity was used to distribute individuals realistically, and individuals then experienced the local conditions (temperature and prey densities) in the channels.

Only the along-channel (x) position was tracked for juveniles and adults. At each 12-h time step, each individual's x position was updated, and its channel or reservoir location was determined. Kinesis represents the distance moved by each individual as the sum of an inertial component (IC) and a random component (RC), with the inertial component dominating when conditions (salinity) are good and the random component dominating when conditions are poor. The position in the x dimension (m from the upstream end of the channel) was updated every 12 h as

$$x_{t+1} = x_t + \Delta x_t \tag{17}$$

and

$$\Delta x_t = IC + RC, \tag{18}$$

where IC is the inertial component that depends on the movement velocity at the last time step (Δx_{t-1}), and RC is the random component based on fish swimming speed.

To compute *IC* and *RC*, we first computed the functions (*f* and *g*) that defined the degree to which salinity (*S*) in the box deviated from optimal salinity,

$$f(S) = H_1 \cdot e^{-0.5 \cdot \left(\frac{S - S_O}{\sigma_S}\right)^2} \quad (19)$$

and

$$g(S) = 1 - H_2 \cdot e^{-0.5 \cdot \left(\frac{S - S_O}{\sigma_S}\right)^2}, \quad (20)$$

where S_O is the optimal value of salinity (2.0 psu); σ_s (= 3.0) determines how quickly the function decreases as salinity deviates from its optimal value; and the *H*-values are constants (0.75 and 0.90) that define the maximum values of the functions. Inertial velocity (*IC*) was then computed using the distance moved in the last time step (Δx_{t-1}) and $f(S)$:

$$IC = \Delta x_{t-1} \cdot f(S), \quad (21)$$

Equation (21) results in the individual moving at the same total velocity (inertial and random combined) as in the last time step to the degree that conditions (salinity) are favorable; $f(S)$ is larger when salinity is near the optimal value (equation 19).

The random component of distance moved (*RC*) was computed based on $g(S)$ and a random component (r):

$$RC = r \cdot g(S). \quad (22)$$

The random component r was calculated as

$$r = N(0, 1) \cdot \frac{d}{2} + d \quad (23)$$

with

$$d = \sqrt{\frac{(0.001 \cdot L \cdot \Delta t \cdot 60 \cdot 60)^2}{2}}, \quad (24)$$

where r is a normal deviate with a mean of d and an SD of $d/2$. The numerator in equation (24) represents the distance (m) moved during one 12-h time step, assuming a swimming speed of 1.0 body length/s. The parameter d computed by equation (24) is typically about 70% of the distance to account for fish not swimming in a straight line. The probability of up-estuary movement (P_{up}) was specified as 0.50; for each individual and each time step, a random uniform number was compared with P_{up} to determine the x direction of movement (seaward or up-estuary) in a channel. The distance moved in that direction was determined by the computed velocity of the individual (Δx_t; equation 18).

If individuals moved past the end of a channel, they then entered a node where they either continued into a new channel or entered a reservoir. The new channel or reservoir was randomly selected from all those connected to the node, regardless of flow (Supplement C). Individuals were simply started at the beginning of a new channel. Supplement D (in the online version of this article) shows the results of testing the behavioral movement with simplified salinity patterns on the model grid.

Up-estuary migrations of adults and seaward migrations of juveniles were simulated using the above kinesis approach by changing S_O (equations 19 and 20) and P_{up}. On December 15 of each year, the spawning migration to freshwater began by changing S_O from 2 to 0 psu and by setting P_{up} to 0.85 (rather than 0.50) so that more moves were in the up-estuary direction. On May 1, the migration of adults and juveniles back to low-salinity water was simulated by setting S_O back to 2 psu and setting P_{up} to 0.15. Once individuals reached their new optimal salinity, P_{up} was switched back to 0.50.

Numerics

We used a super-individual approach (Scheffer et al. 1995) in order to accurately simulate the addition of new yolk sac larvae each year while ensuring that we did not exceed computer limitations (Supplement E in the online version of this article). Each super-individual represented some number of identical individuals in the population, which we term its "worth." Each year during spawning, the same number of super-individuals was added, but with their initial worth adjusted to reflect the yolk sac larvae produced. Mortality acted to decrement the worth of an individual, with the worth then being used to determine population-level numbers of eggs spawned and Delta Smelt densities and abundances. We used a complicated algorithm for determining how to allocate the fixed number of super-individuals each year among hatch dates and boxes (Supplement E). In all simulations, we used 150,000 super-individuals per age-class (450,000 super-individuals total) because this was sufficient for convergence (i.e., almost identical results were obtained when we followed more super-individuals). The model was coded in FORTRAN90.

Computation of Population Growth Rate

We used the individual-based model output to estimate a simple Leslie age-based matrix model for each year, which allowed us to summarize the multidimensional individual-based model results with a single variable of annual finite population growth rate (λ). The value of λ was based on the detailed dynamics of the individual-based model but allowed for easier comparison among years. A 2×2 matrix model was estimated for each year by computing the average maturity, fecundity, and age-specific survival rates (Supplement F in the online version of this article); eigenvalue analysis was then used to determine λ. The value of λ for a specific year is a measure of the conditions for Delta Smelt during that year. The λ value is also a reflection of conditions from the previous year by indicating how growth in the fall prior to spawning affected the elements related to maturity and fecundity in the matrix.

TABLE 2. Calculation of the major model output variables examined in Delta Smelt model simulations and the calculations for the data when model–data comparisons were performed. The corresponding figures for the results are noted; "text" means the results are described in the text.

Variable	Model calculations	Data calculations
(a) January adult abundance (Figure 5)	Summed worth of all individuals on January 1; includes young of the year that just became age 1 and age-1 fish that just became age 2 but does not include age-2 fish that were just removed as they became age 3.	Catch per trawl from the spring Kodiak trawl survey for 2002–2006 was averaged for January and February (first two trawls) and expanded to population size using volume sampled, 100% efficiency, and volume of Sacramento–San Joaquin Delta and Suisun Bay less than 4 m deep. November and December midwater trawl (MWT) abundance was computed the same way but by using volume of Delta and Suisun Bay less than 4 m deep. Log(Kodiak trawl abundance) was then regressed against log(MWT abundance), and the MWT values were used to estimate Kodiak trawl values for 1995–2001.
(b) Mean length of young-of-the-year, age-1, and age-2 fish (Figure 6)	Computed the weighted mean lengths on January 1 (just before their birthdays) using worth as the weighting factor in the averaging.	Mean length of fish in the December MWT samples, excluding fish greater than 100 mm, which were assumed to be age 1 or older.
(c) Annual number of adults entrained in diversion facilities (Figure 7)	Summed worth of individuals that were killed by arrival at reservoir 4 (State Water Project) or node 181 (Central Valley Project), plus the worth associated with the added mortality of all individuals in box 3 (South Delta) when Middle River flow is negative. The amount of worth (w) attributable to Middle River-related mortality (R) versus natural mortality (M) is $w(\frac{R}{M+R})(1 - e^{-M+R})$.	Methods are described by Kimmerer (2008), and results used here are shown in Figure 12a of that paper.
(d) Fraction of adults on January 1 subsequently entrained during that year	Ratio of numbers entrained (see variable c) divided by the January adult abundance (see variable a)	Methods are described by Kimmerer (2008), and results used here are shown in Figure 12c of that paper.
(e) Fraction of age-1 individuals that were mature and the number of eggs per entering age-1 individual (Figure 8)	Fraction mature was computed as the summed worth of age-1 individuals greater than 60 mm at the time of projected spawning divided by the summed worth of all age-1 individuals on the same day. The ratio of eggs to entering age-1 fish was computed as the cumulative number of eggs produced by age-1 individuals divided by the summed worth of age-1 fish on January 1 prior to spawning.	No data.
(f) Salinity weighted by densities of larvae, juveniles, and adults (Figure 9)	First, the worth of larvae (including postlarvae) was summed for each box on each day and then divided by the volume of the box to obtain number per m^3 by box on each day. Salinity in each box on each day was used to compute average salinity across boxes, weighted by the larval densities in each box. This process was repeated for juveniles and for adults. This was done for calendar years to better match following a year-class from the early spring spawning.	Number per trawl in each sample of the 20-mm, summer townet, fall MWT, and spring Kodiak trawl surveys was used to weight the salinity value measured with the trawls. Data values include a mix of larvae, juveniles, and adults that varied throughout the year depending on the survey.
(g) Proportion of individuals in and seaward of the confluence box for adults on December 14 and April 30, for postlarvae on June 24, and for juveniles and adults on September 1 (Figure 10)	For each stage and day, we summed the worth of individuals in each box and then divided the sum of worth in the confluence box and seaward boxes by the total summed worth over all boxes.	All of the fall MWT data from all stations during September–December were aggregated for each year, assigned to up-estuary of the confluence box (47 stations) or in or seaward of the confluence box (39 stations). The proportion in Figure 10f was computed from these two totals.

TABLE 2. Continued.

Variable	Model calculations	Data calculations
(h) Daily fraction of larvae plus postlarvae entrained in diversion facilities (Figure 11)	Summed worth of larval and postlarval individuals reaching reservoir 4 and node 181 divided by the summed worth of larvae and postlarvae at the end of the day plus the numbers lost to pumping plant entrainment during that day.	Methods are described by Kimmerer (2008), who used the 20-mm survey data, and the results are shown in Figure 14 of that paper. Note: Kimmerer's (2008) estimates included some juveniles as well as larvae and postlarvae. Also see recent papers about the estimation by Kimmerer (2011) and Miller (2011).
(i) Diets (text)	Computed averaged diets for each life stage using the biomass of zooplankton types eaten by every 500th individual on every 30th day. We first computed the proportions for each individual and then averaged the proportions over individuals. This resulted in individuals covering all life stages for the time periods during which the stages were present.	Diets reported by Lott (1998), Nobriga (2002), and Baxter et al. (2010), who summarized unpublished data from Steven Slater (California Department of Fish and Game); data were only sufficient for qualitative and general comparison.
(j) Annual finite population growth rate (λ; Figure 12)	The λ value was computed from a 2×2 Leslie matrix model with parameter values determined from the individual-based model output each year (see Supplement F).	No data.
(k) Stage-specific survival rates (Figure 13)	Summed worth of individuals entering each life stage during the year divided by the summed worth of individuals entering the next life stage.	No data.
(l) Averaged temperature and proportion of maximum consumption (p-values; text)	Computed average temperature and average p-value for all individuals (weighted by their worth) each day and then computed seasonal averages weighting the daily values for total daily worth of age-1 individuals during February 27–June 7 (spawning) and total daily worth of juveniles during April 18–October 1 (growing season) and October 1–December 30 (fall).	

MODEL SIMULATIONS

Calibration

The model was calibrated in three steps. We first tested the movement of juveniles and adults on test grids with fixed salinity patterns to understand movement in contrived situations where we knew the correct movement patterns (Supplement D). Once the entire model had been calibrated, we again evaluated the movement patterns among years to confirm that simulated movement was realistic under dynamic salinity conditions. The results using the full model are presented below as part of the 1995–2005 historical simulation.

The second step was to determine the K-values (equation 10) for each Delta Smelt life stage and each zooplankton prey group (Supplement B). We averaged daily temperature and the biomass of each zooplankton group in each box over the periods when each life stage would be in the system. We assumed that larvae, juveniles, and adults remained in each of the 11 boxes, and we then iteratively adjusted the K-values so that the average consumption rate (i.e., with p-value $= 0.8$) and diets were reasonably close to the available observations.

The third and final step was to put the above two calibrated components (movement and growth) into the full model and then to simulate the period 1995–2005 by adjusting only the yolk sac larval mortality rate and the entrainment mortality multiplier based on Middle River flow. The mortality rate of yolk sac larvae was adjusted because this mortality was relatively simple (i.e., only temperature dependent and of short duration). The entrainment mortality multiplier was adjusted because the role of Middle River flow in affecting entrainment is well documented (Grimaldo et al. 2009), although the magnitude is uncertain, and we had data on adult entrainment mortality (Kimmerer 2011). We adjusted the yolk sac larval mortality rate until the predicted average January abundance for 1995–2005 was close to the data average of 2.7×10^6; we then adjusted the entrainment mortality multiplier until the average annual fraction of adults removed by diversions was close to the data average of 10%. We did not try to fit to individual years or to the pattern in the time series of annual abundances. Thus, any interannual differences in model output were generated by differences in temperature, salinity, entrainment, and zooplankton densities.

Historical Simulation

We report the results from the last step of the calibration: the 1995–2005 historical simulation. The calculations that were performed to obtain all reported model outputs and to summarize the field data used for model–data comparisons are shown in Table 2. The field data for Delta Smelt originate mostly from four surveys that are conducted annually by the California Department of Fish and Game (www.dfg.ca.gov/delta/): (1) the fall midwater trawl (MWT) survey began in 1967 and samples juveniles and adults monthly during September–December at 116 stations; (2) the spring Kodiak trawl survey began in 2002 and samples adults every 2–4 weeks during winter and spring at 39 stations; (3) the 20-mm survey (larval net) began in 1995 and samples larvae at 48 stations between March and July; and (4) the summer townet survey began in 1959 and samples mostly juveniles at up to 32 stations during June–August. These field data have been described and used extensively in previous analyses (e.g., Bennett 2005; Kimmerer et al. 2009; Sommer et al. 2011; Miller et al. 2012).

The model outputs and the model–data comparisons in Table 2 confirmed various aspects of the calibration or served to assess the realism of model behavior. None of the model–data comparisons can be considered as true model validation because no data were kept aside for independent comparison. Comparisons a–d in Table 2 were related to the three steps in model calibration as described above. Maturity of age-1 individuals and the number of eggs per entering age-1 individual (Table 2, comparison e) integrated the effects of growth differences (due to temperature and prey biomass) from the previous year on reproduction. Movement patterns were confirmed by using averaged salinities weighted by Delta Smelt density (comparison f) and the proportions of individuals in and seaward of the Sacramento River–San Joaquin River confluence box (comparison g). We used monthly Delta outflows (m^3/s) from DAYFLOW (www.water.ca.gov/dayflow/) to help interpret the spatial distributions in comparison g. Comparison h, the daily fraction of larvae lost to entrainment, confirmed the realism of the pumping-related mortality determined by the PTM. Overall average diets (comparison i) were examined to confirm reasonable shifts in diet from larvae to juveniles to adults. The λ values (comparison j) and stage survival rates (comparison k) provided condensed summaries of the differences among years. Finally, comparison l identified the between-year differences in temperature and food as actually experienced by the simulated fish.

MODEL RESULTS

Dynamics within the Historical Simulation

For the simulated period 1995–2005, calibration resulted in an average January adult abundance of 2.7×10^6 (compared to the data target of 2.3×10^6) and an average fraction of adults lost to the pumps of 11% (the target was 10%). The final calibrated mortality rates were 0.035 d^{-1} for yolk sac larvae and 0.02 d^{-1} for Middle River-related pumping mortality. Annual January abundances varied from year to year in a pattern similar to that of data-based estimates, with a peak in 2000, a decline in 2001, and then low abundances in 2002–2005 (Figure 5). One exception was that the January adult abundance in 1996 had the highest data-based estimate but a relatively low simulated value.

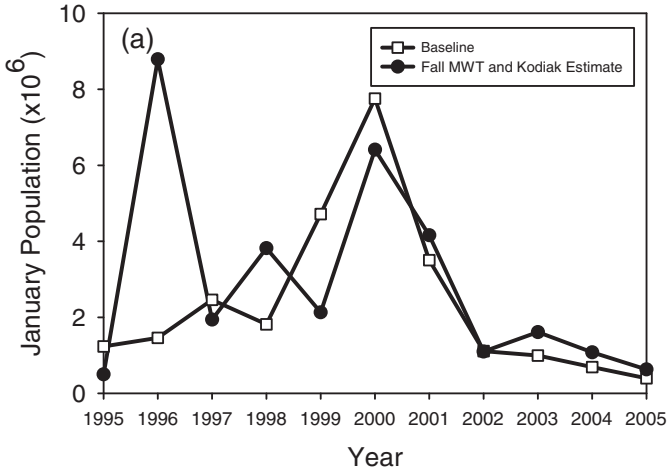

FIGURE 5. Annual abundance of adult Delta Smelt in January for 1995–2005 from the baseline simulation and as estimated from the fall midwater trawl (MWT) and spring Kodiak trawl sampling.

Simulated lengths at age on January 1 were similar to data values for young of the year about to become age 1, with both model and data values varying between 55 and 65 mm (Figure 6). Faster growth was predicted for the summer and fall of 1995 (shown as the January 1996 value), 1997 (the January 1998 value), and 2001–2004. Simulated growth was slow in 1996, 1999, and 2000, resulting in shorter fish recorded during the

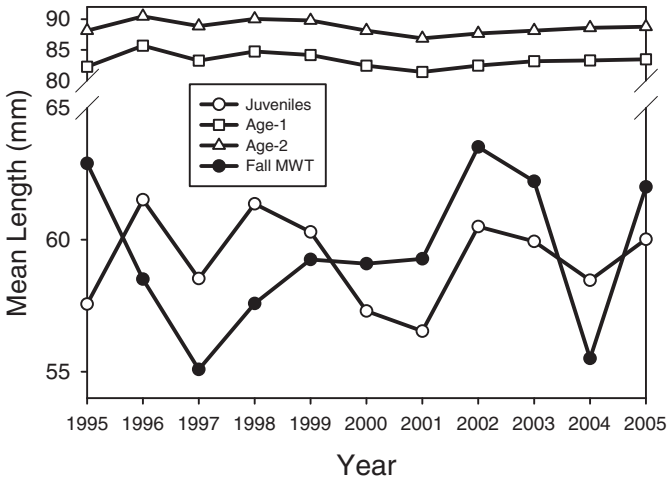

FIGURE 6. Mean total length of juvenile, age-1, and age-2 Delta Smelt on January 1 in each year (just prior to birthdays) of the 1995–2005 baseline simulation. Also included are the mean lengths of young-of-the-year fish from fall midwater trawl (MWT) sampling.

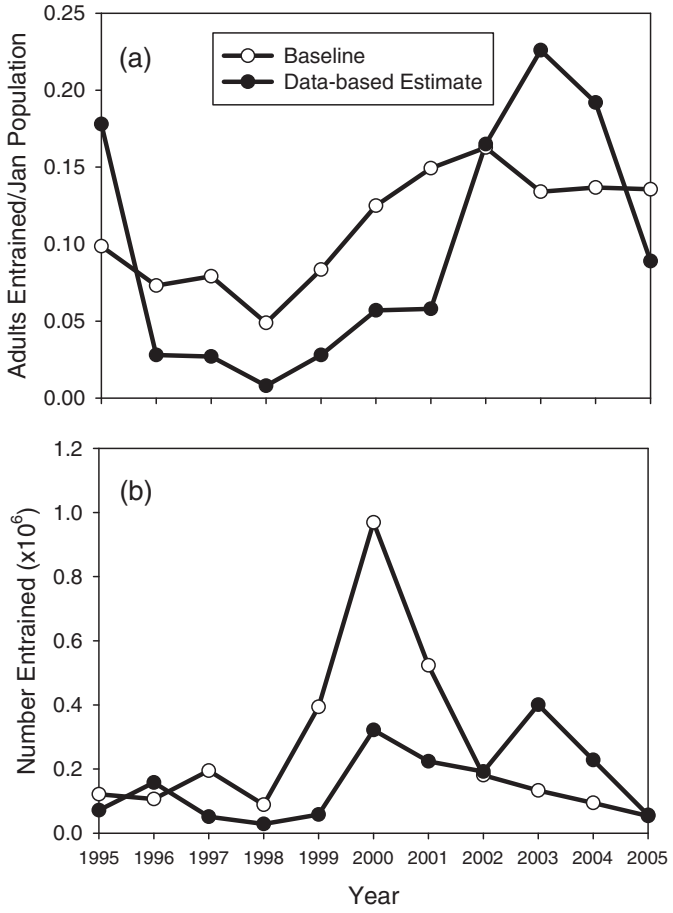

FIGURE 7. Predicted and observed annual values in 1995–2005 for **(a)** the fraction of adult Delta Smelt present in January that were entrained in pumping plants during the next few months (i.e., winter) and **(b)** the number of adults that were entrained during the same time period.

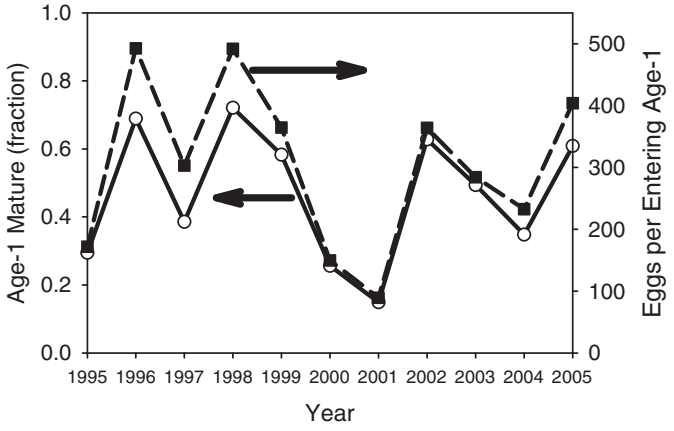

FIGURE 8. Annual fraction of age-1 individual Delta Smelt that were mature (solid line, open circles) and the number of eggs produced per entering age-1 individual (dashed line, black shaded squares) for the 1995–2005 baseline simulation.

next January. Mean lengths of about 82 mm for age-1 fish (about to become age 2) and 90 mm for age-2 fish (about to become age 3) were consistent with the results of Bennett (2005).

The predicted annual fraction of adults entrained showed less interannual variation than the data-based values (Figure 7a), and the predicted numbers entrained were as much as two times the data values for 1999–2001 (Figure 7b). Predicted and estimated annual fractions entrained were low (<10%) for 1996–1999 and then increased to 15–20% for 2002–2004. Predicted fractions showed less variation and were higher than estimated values during the earlier, low-entrainment-loss years and were lower than estimated values during the latter, high-entrainment-loss years (i.e., in Figure 7a, the line connected by open circles is flatter than the line connected by black shaded circles). Substantially more model adults were entrained during 1999–2001 than were shown by the data (Figure 7b) because the fraction entrained was higher, and in two of those years the population estimate (Figure 5a) was higher than that in the data. Overestimation of the fraction entrained in early years and underestimation of the fraction entrained in later years suggested inaccuracies in the simulated adult spatial distributions or in the use of a single value for the pumping mortality at any southward Middle River flow.

Even though the variation in mean length of age-1 adults was small (± 5 mm; Figure 6), interannual differences had large effects on maturity (Figure 8, solid line) and subsequent egg production (Figure 8, dashed line) by age-1 individuals. Age-1 individuals at the beginning of the spawning season (about 3 months into age 1) varied above and below 60 mm from year to year. This hovering around 60 mm caused the fraction of age-1 fish that were mature to range from 0.15 (in 2001) to 0.60–0.70 (in 1996, 1998, and 2002; Figure 8), tracking the slow and fast age-0 growth from the previous year (Figure 6). A greater fraction of individuals becoming mature and a higher weight of these individuals (equation 1) resulted in a fivefold difference among years in the number of eggs produced per entering age-1 individual (Figure 8). Egg production per entering age-1 fish was highest in 1998 (491.8) due to the fast growth of juveniles in 1997 and the high proportion (72%) of age-1 fish being mature at spawning; egg production per entering age-1 individual was lowest in 2001 (89.3; 15% maturity) due to slow juvenile growth in 2000. Such large variation in the fraction mature and eggs produced per entering age-1 fish seems extreme and may partially reflect the all-or-none maturity rule (100% mature if longer than 60 mm) we used. We further investigate the maturity rule in our companion paper (Rose et al. 2013).

Simulated Delta Smelt density-weighted salinities showed the up-estuary spawning migration of adults and the subsequent larval and juvenile movement seaward (Figure 9). Note that the years in Figure 9 are calendar years (i.e., they start on January 1) in order to follow a year-class. Salinity slowly rose for larvae and postlarvae during June–September as they were transported seaward (Figure 9a). Salinity also rose for juveniles during June–October (Figure 9b) after the S_O for juveniles was changed from 0 to 2 psu on May 1. Salinity for adults went from near zero in January–May to approaching 2–6 psu beginning in June

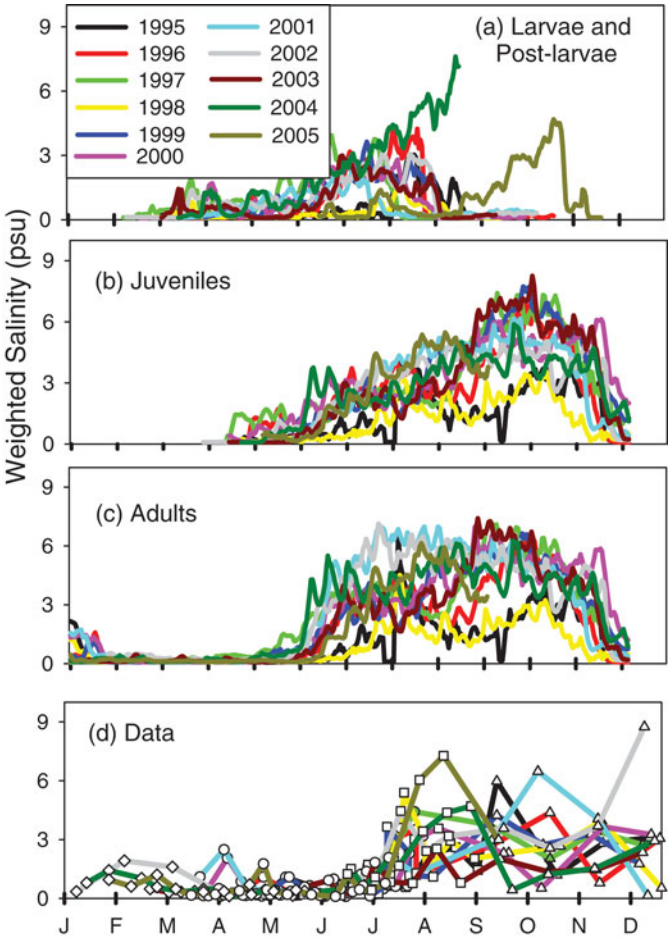

FIGURE 9. Average salinity (psu) weighted by Delta Smelt density computed daily during calendar years 1995–2005 for **(a)** larvae and postlarvae combined, **(b)** juveniles, and **(c)** adults in the baseline simulation. Panel **(d)** shows the weighted salinity values obtained by merging catch per unit effort data from the 20-mm, summer townet, fall midwater trawl (MWT), and spring Kodiak trawl surveys for 1995–2005. Years are calendar years rather than water years (e.g., 1997 refers to January–December). [Figure available online in color.]

(Figure 9c), triggered by a change in the adults' S_O back to 2 psu on May 1. During most years, the density-weighted salinity values for juveniles and adults caused their seaward migration to occur earlier than was shown in the data (June in Figure 9c versus 9d), and they occupied water during the late summer and fall with salinities of 2–6 psu, whereas the data suggested somewhat lower-salinity waters of 1–4 psu during the late summer and fall (August–October in Figure 9c versus 9d).

The interannual influence of Delta outflow on the proportion of individuals in each spatial box is shown in Supplement G (in the online version of this article) and is summarized here by using a single metric: the proportion of fish that were within or seaward of the confluence box (Figure 10). In December, prior to their up-estuary spawning migration, adults were distributed based on salinity, which was roughly correlated with average October outflow (Figure 10a). During the high-outflow years of 1996 and 1999, more than 80% of adults were in or seaward of the confluence box, whereas during the remaining years fewer than 60% were in or seaward of the confluence box.

Spawning migration (including young-of-the-year fish that became age 1 on January 1) began in January and ended by April 30, with almost all individuals located up-estuary of the confluence box (Figure 10b). Once hatched, larvae were transported by the PTM; by June 24, when postlarvae were about to become juveniles, proportions again roughly reflected outflow conditions (Figure 10c). During 1995 and 1998, which were years of high May outflow, over 80% of postlarvae were in or seaward of the confluence box, whereas during relatively low-outflow years (2001, 2002, and 2004) only 20–30% of postlarvae were located in or seaward of the confluence box. Data for 1997 appear anomalous relative to May outflow because that year had a low May outflow but the highest June outflow over the simulation time period (2,033 m^3/s versus less than 1,327 m^3/s). Juvenile and adult distributions on September 1 (Figure 10d, e) resembled each other because both reflected behavioral movement towards 2-psu water. Juveniles and adults were farthest seaward during the high outflow of August 1998 and were situated up-estuary during the low-outflow years of 2001, 2002, and 2004.

Finally, the predicted and observed proportions of adults that were in or seaward of the confluence during the fall showed moderately good agreement for extremely low- and high-outflow years but not for years of intermediate flow (Figure 10f). Predicted and observed proportions showed relatively more fish in and seaward of the confluence during 1996 and 1999 and more fish being relatively up-estuary during 1995, 2004, and 2005. October outflow was highest in 1996 and 1999 and was low in 1995 and 2004 (Figure 10a); October outflow for 2005 was not low, but the summed October–December outflow in 2005 was relatively low. However, predicted proportions were flatter than observed proportions (proportions under low outflow were above the 1-to-1 line, and proportions under high outflow were below the 1-to-1 line in Figure 10f), indicating that simulated adults were generally too far seaward under low outflow and too far up-estuary under high outflow.

The simulated daily proportion of larvae and postlarvae entrained, which results from transport by the PTM, generally agreed with the data-based estimates (Figure 11). Model predictions showed less interannual variation than the data-based values. A few extreme model values of 0.2–0.3 were predicted, whereas data values never exceeded 0.1. In both the simulation and in the data, entrainment was relatively low during 1995, 1996, and 1998 and was high during 2002 and 2003. Model-predicted entrainment was also high during 2000, 2001, and 2005, which were intermediate entrainment years in the data.

Simulated diets were reasonable and consistent among years, even between the most extreme years (not shown). Larvae consumed *Limnoithona* spp. (20% of consumed biomass) and calanoid copepodids (80%) because other prey had vulnerabilities of zero. As Delta Smelt increased in size, they consumed

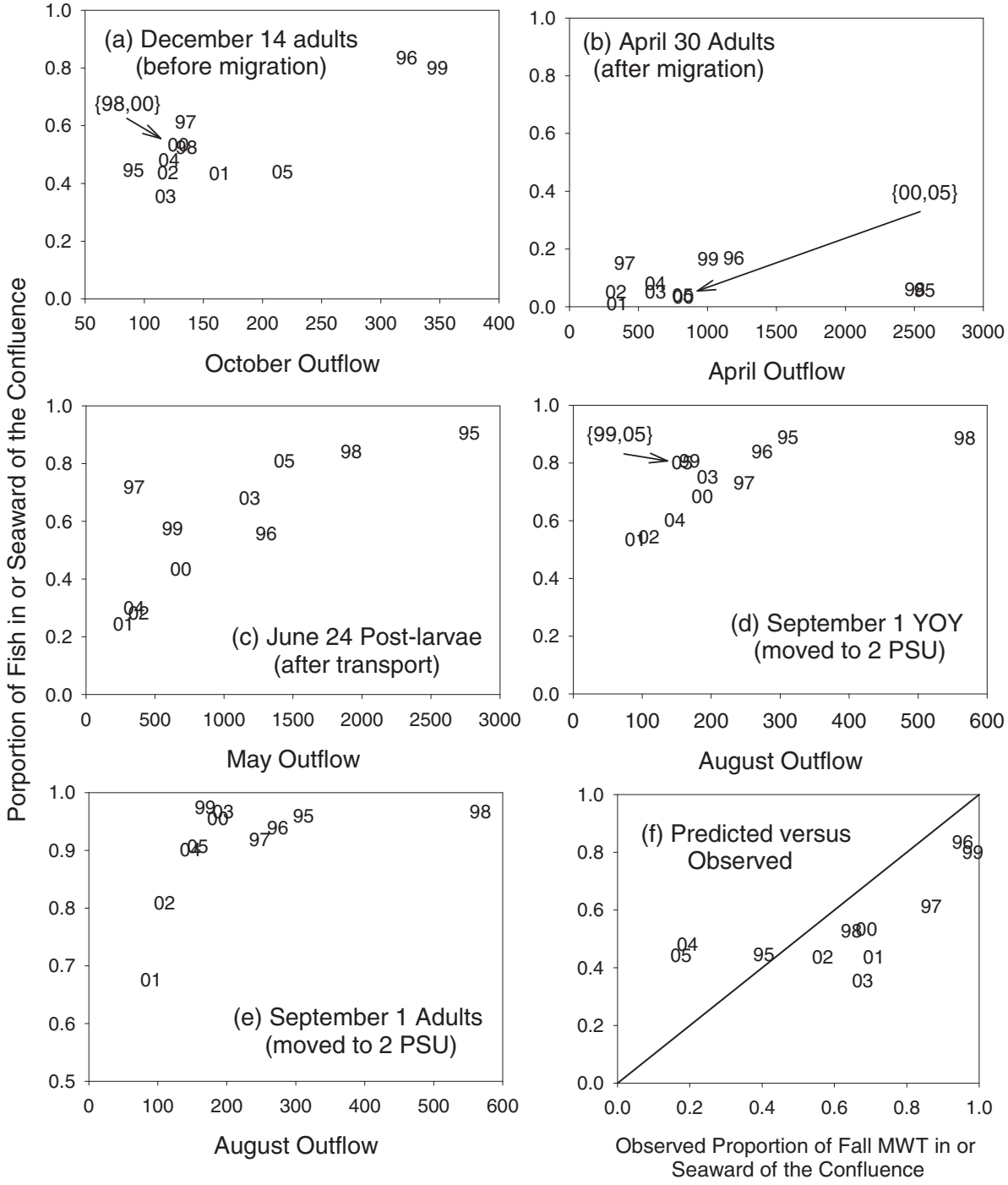

FIGURE 10. Predicted proportion of Delta Smelt individuals in the confluence and seaward boxes (see Figure 1) versus monthly Sacramento–San Joaquin Delta outflow (m^3/s) in the immediately preceding months for 1995–2005 of the baseline simulation: **(a)** adults on December 14 (before the spawning migration), **(b)** adults on April 30 (after the spawning migration), **(c)** postlarvae on June 24 (after particle tracking model transport), **(d)** juveniles (young of the year) on September 1, and **(e)** adults on September 1. Two-digit numbers indicate water years (e.g., 96 = 1996; 02 = 2002). Panel **(f)** is a comparison of the predicted proportion of Delta Smelt in and seaward of the confluence box from December 14 versus the proportion estimated from the fall midwater trawl (MWT) survey. Panel (a) uses outflow from October of the previous year (e.g., October 2001 outflow for the year 2002).

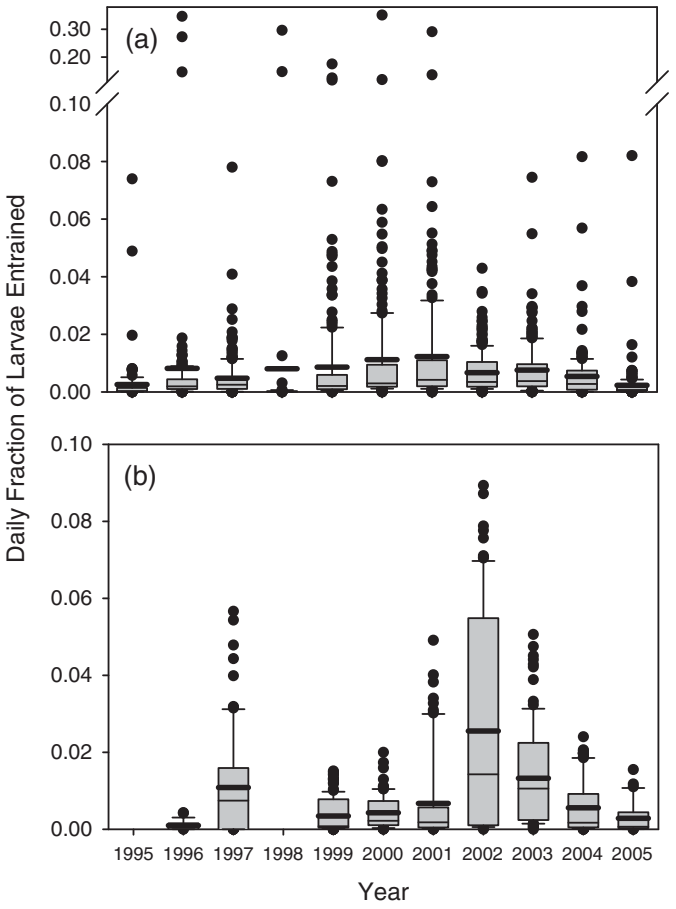

FIGURE 11. Daily entrained fraction of **(a)** Delta Smelt larvae and postlarvae combined as determined by the particle tracking model for 1995–2005 of the baseline simulation and **(b)** larvae (and some juveniles) as estimated by Kimmerer (2008). The thin line within each box is the median, the thick line is the mean, the ends of the box represent the 25th and 75th percentiles, the ends of the whiskers represent the 10th and 90th percentiles, and the black circles are points outside of the 10th and 90th percentiles.

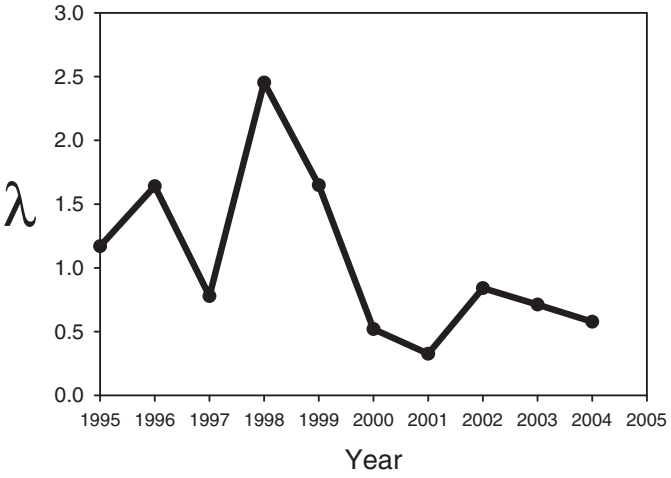

FIGURE 12. Population growth rate (λ; fraction per year) of Delta Smelt as determined by the age-based Leslie matrix model applied to individual-based model output for each year of the 1995–2005 baseline simulation. No value for 2005 was possible because the simulations ended on September 30, 2005; information through December 31, 2005, would be needed to estimate the matrix model for 2005.

less *Limnoithona* spp. and calanoid copepodids and more of the other four adult zooplankton types (50% [*Limnoithona* spp. and calanoid copepodids] and 50% [other types] for postlarvae; 79% and 21% for juveniles; 92% and 8% for adults). *Pseudodiaptomus* increased in the diet as fish transitioned from postlarvae to juveniles, but the *Pseudodiaptomus* contribution then decreased slightly between juvenile diets and adult diets as the biomass of this zooplankton type decreased in the fall. These results qualitatively agreed with several diet studies of Delta Smelt (Table 2), but more rigorous comparison was not attempted because of the difficulties in interpreting field diets involving rapidly digested zooplankton and without simultaneous measurement of zooplankton densities.

Best versus Worst Years in the Historical Simulation

Population growth rate (λ) from the Leslie matrix model showed that water year 1998 was the best year and water year 2001 was the worst year for the simulated Delta Smelt population (Figure 12). The λ in each year resulted from a combination of (1) growth in the prior year affecting subsequent reproduction and (2) higher stage-specific survival rates in the current year for most of the life stages. Thus, water year 1998 extended from October 1997 to September 1998 and included the fall of 1997, which led up to spawning in spring 1998. Fast growth in fall 1997 resulted in large new adults at the beginning of 1998 (Figure 6) and therefore a high fraction of mature age-1 fish and a high number of eggs per entering age-1 individual (Figure 8). The year 1998 also had moderately high growth during summer (Figure 6), the lowest entrainment losses (Figure 7a, 11), and the highest stage-specific survival rates for all life stages (Figure 13). The bad year, 2001, had the second slowest growth in the prior year (2000; Figure 6) and consequently had the lowest number of eggs per entering age-1 fish (Figure 8). In addition, 2001 had moderately high entrainment losses (Figure 7) and low survival of eggs (Figure 13a), juveniles (Figure 13e), and adults (Figure 13g, h).

Compared with 2001, water year 1998 had a relatively cool and delayed warming in spring that benefited Delta Smelt larvae, but both years had similar growth conditions for juveniles during summer. Mean temperature experienced by age-1 individuals during February 27–June 7 (spawning) was 14.8°C in 1998 versus 16.4°C in 2001. Average day of spawning was April 28 in 1998 versus April 6 in 2001, and average duration of the larval stage (inversely related to growth rate) was 25.2 d (1998) versus 28.6 d (2001). Although juveniles also experienced cooler temperatures during the early summer (16.7°C versus 22.2°C for April 18–June 7), differences became smaller when viewed over the entire growing season. Average temperature experienced by juveniles during April 18–October 1 was slightly cooler during 1998 than during 2001 (20.9°C versus

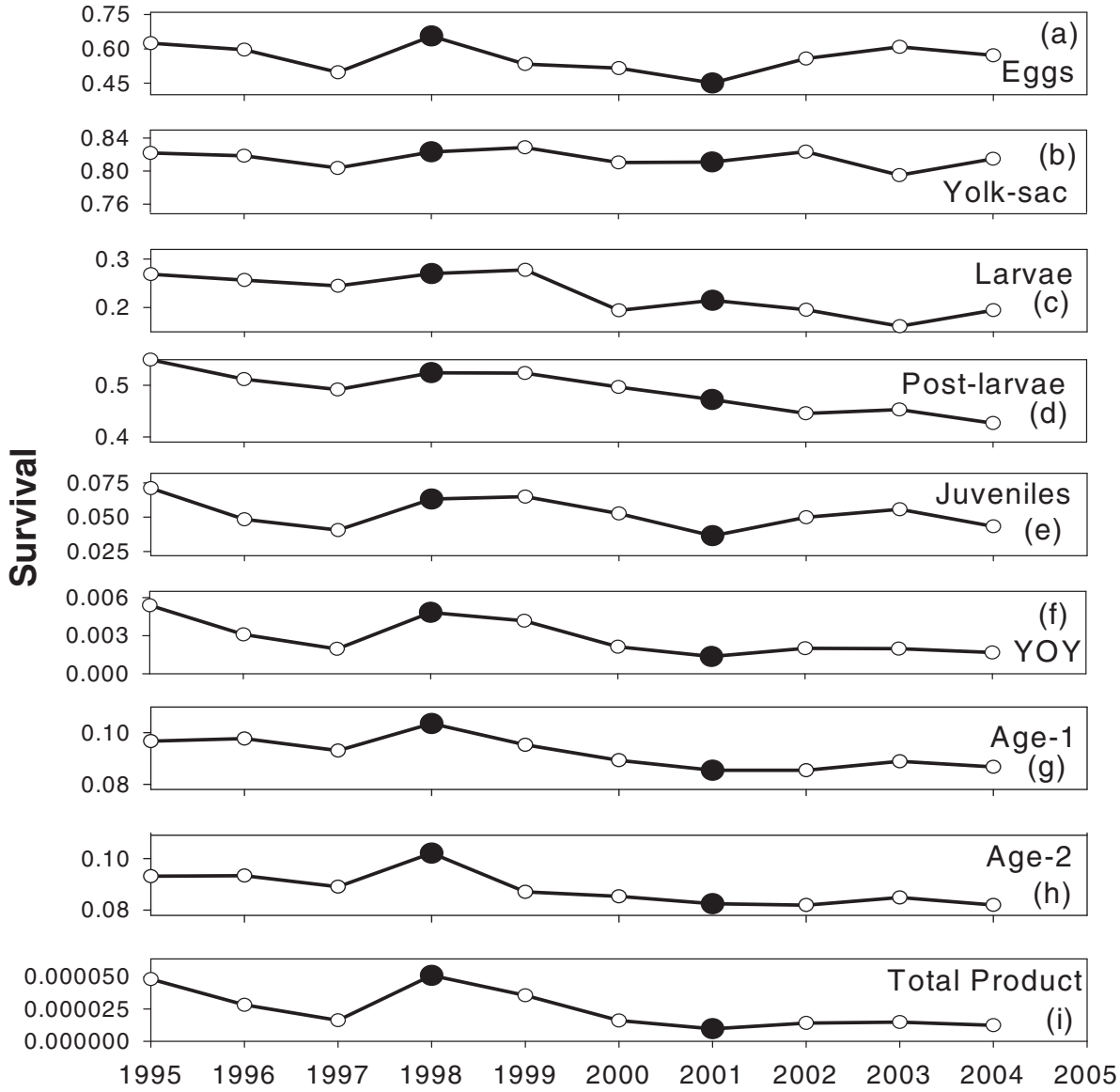

FIGURE 13. Delta Smelt stage-specific survival (fraction) from the 1995–2005 baseline simulation for **(a)** eggs, **(b)** yolk sac larvae, **(c)** larvae, **(d)** postlarvae, **(e)** juveniles, **(f)** total young of the year (product of a–e), **(g)** age 1, **(h)** age 2, and **(i)** total (product of f–h).

22.1°C), and the average *p*-value was higher in 1998 (0.89 versus 0.84). However, mean lengths of juveniles were similar between 1998 and 2001 (60.3 mm in 1999 versus 60.5 mm in 2002; Figure 6), so the difference in summer growth of juveniles between 1998 and 2001 was not a major factor.

The higher number of eggs per age-1 individual in 1998 compared with 2001 was due to faster growth during fall 1997 compared to fall 2000. Mean length of juveniles on January 1 (just before their birthday to age 1) was 61.4 mm for 1998 versus 56.5 mm for 2001. The mean *p*-value for October 1–December 30 was 0.76 in 1997 versus 0.68 in 2000; 1997 was also warmer than 2000 (15.9°C versus 15.0°C).

Delta outflow was generally higher in 1998 than in 2001 (Figure 10), so individuals were farther seaward, resulting in lower entrainment mortality during 1998. The PTM put 84% of postlarvae in or seaward of the confluence box on June 24 in 1998 compared with 24% on June 24 in 2001 (Figure 10c). Similarly, behavioral movement of juveniles resulted in about 88% of them occurring in or seaward of the confluence box on September 1, 1998, versus 53% on September 1, 2001 (Figure 10d). Almost no larvae were predicted to be entrained during 1998, whereas a daily average loss of 1.2% was predicted for 2001 (Figure 11a); the fraction of January adults entrained was 0.05 in 1998 versus 0.14 in 2001 (Figure 7a).

DISCUSSION

We used a detailed, individual-based approach to model the population dynamics of Delta Smelt during a time period that included a major population decline. The model was completely density independent; a density-dependent version is analyzed by Rose et al. (2013). The Delta Smelt has been declining since the 1980s and was one of four species to show a step decline around 2002 (Sommer et al. 2007). The choice of a detailed individual-based model may seem odd because of the extensive data demands of this general approach. Survey data-based modeling approaches are easier to justify in terms of calibration and in testing the degree of fit (e.g., Thomson et al. 2010; Miller et al. 2012); however, unlike our process-based approach, survey data-based approaches do not provide a means of assessing cause-and-effect relationships and so far have not helped to settle the controversy over the causes of the decline.

We opted for a spatially explicit, individual-based approach to explore the potential causes for the Delta Smelt's decline and the conditions that result in good versus bad years for Delta Smelt. The term "spatially explicit" refers to multiple, linked spatial boxes with different conditions among them. The individual-based approach allows for relatively easy simulation of movement and for local experiences to accumulate as each individual moves among the spatial boxes. A spatially explicit approach was required to enable a model that could (1) represent feeding, growth, reproduction, and movement in some detail; and (2) simulate how interannual variation in spatial distributions by life stage interacted with dynamic habitat. The chief disadvantage of such a complicated mechanistic model is that describing how it works can be difficult (Grimm et al. 2006), and many of the assumptions and parameter values must be based on judgment; thus, replication of the modeling by others is a challenge (Wilensky and Rand 2007). Indeed, the output of our model was sufficiently complicated that we chose to fit an age-structured matrix model to its output to provide a more straightforward summary of each year's condition. Our model is designed for exploring hypotheses about some of the factors affecting Delta Smelt population dynamics but is not designed for forecasting future Delta Smelt population abundances. Hypotheses about future conditions can be explored with our model but in a relative way, whereby simulated values are compared with some simulated baseline condition.

Maunder and Deriso (2011) also fitted a stage-based model of Delta Smelt by using the same extensive long-term monitoring data used here. By including covariates such as annual entrainment rate in their model, Maunder and Deriso (2011) were able to evaluate the relative importance of different factors. Their data-based modeling approach is relatively easy to describe (mathematically compact) and can be easily judged for its performance and skill (fit to data), but the approach also inherits problems with the monitoring data in terms of bias and process versus observation errors and is heavily correlation based. Clearly, the data-based approach of Maunder and Deriso (2011) and the detailed, process-based approach used here can complement each other, and detailed comparison between the two approaches would likely allow for more insights than either approach alone can provide.

Calibration of complicated individual-based models is always a challenge. Our approach was first to adjust the movement and feeding algorithms externally under simplified conditions and then calibrate by adjusting two mortality-related parameters for the 1995–2005 historical simulation to get the averaged population abundance and averaged fraction entrained to match the data. None of the calibration steps involved adjustments to fit the model to specific years.

Model results were generally consistent with the available data and information (Table 2) about Delta Smelt. The model reasonably matched a variety of measures related to growth, mortality, and movement. Predicted growth resulted in realistic lengths at age (Figure 6). The PTM produced reasonable larval entrainment rates (Figure 11), and a simple function of Middle River flow yielded annual adult entrainment fractions that mimicked the observed values (Figure 7). Movement was confirmed both based on salinity experienced by individuals (Figure 9) and geographically (Figure 10). The fraction of individuals in the confluence box and seaward boxes during the fall agreed with estimates from fall MWT sampling. Thus, the calibrated model is a good descriptor of the 1995–2005 conditions and is useful for comparing Delta Smelt dynamics among those years. We caution that our bioenergetics model was sufficient for relating prey and temperature to growth, but it must be re-evaluated for other purposes.

There were several major discrepancies between model results and observed values. First, the model underestimated the January abundance in 1996 (Figure 5), and the reason for this is unclear. Second, the model overestimated the degree of adult entrainment in early years and underestimated the degree of adult entrainment in later years (Figure 7). This lack of sufficient interannual variation in simulated adult entrainment may be attributable to the simulated movement of adults being too similar among years (Figure 10f); the center of distribution for simulated adults was less variable across years than the center of distribution for fish caught by the fall MWT. Another possible explanation is that adult entrainment mortality was switched on or off depending on the sign of Middle River flow, whereas analyses showed that the actual entrainment rate probably increases with the magnitude of southward flow toward the diversion facilities (Kimmerer 2011).

A third discrepancy between the model and the data was that movement in the model tended to put juveniles and adults in water that was too saline during late summer to winter (Figure 9). This could reflect a conceptual difference between the data-based and modeled density-weighted salinities. Because the model tracks each individual, an individual-weighted salinity is unbiased by any sampling error. In contrast, the sampling programs catch relatively few fish and do not sample all salinities equally. However, even with the sampling issues, the results suggest that the model is contributing to this discrepancy. Two

possibilities are that (1) behavioral movement of juveniles in the model may be too slow to react to local salinity changes (Supplement D) and (2) the starting locations from the PTM were too far seaward. Some of the movement of late larval Delta Smelt in nature likely is a result of both transport (which we assumed) and behavior as the fish gain competence to direct their movements.

Finally, the model showed wide fluctuations in the fraction of age-1 individuals that were mature and the number of eggs per entering age-1 individual (Figure 8) from small changes in mean length (Figure 6). Although we lack data with which to compare these results, these differences among years seemed larger than what we would expect to see in the real population. We partially address this in Rose et al. (2013) by including length-dependent maturation as one of the alternative baselines.

We performed many comparisons of model results with the available data (Table 2), but we did not perform the classical model calibration and validation comparisons and we did not compare model predictions with commonly used abundance indices from the monitoring programs. We focused on using most of the data for calibration and often in a pattern-matching mode (Grimm et al. 2005) rather than a more traditional comparison of predicted values versus observed data (Stow et al. 2009); thus, some of the consistency between the model and the data was a result of calibration. While Delta Smelt abundance indices from the various monitoring programs have been used extensively as indicators of population abundance and survival (Bennett 2005; Maunder and Deriso 2011; Miller et al. 2012), we found the model–data comparisons using the indices to be uninformative due to the sensitivity of the indices to calculation details, such as the months included and the gear selectivity (e.g., Newman 2008).

Our analysis of model results and data for 1995–2005 clearly illustrated why it has been difficult to ascribe the Delta Smelt's decline to a single causative factor, either over the long term or as part of the recent 2002 decline. Interannual variation in λ (Figure 12) was due to a combination of the effects of temperature, salinity, larval growth, hydrodynamics, and growth of juveniles in the prior year affecting the movement, growth, mortality, and reproduction in various combinations of life stages. Small changes in mean length of young-of-the-year fish from the previous year (Figure 6) were amplified into large effects on egg production (Figure 8), and temperature affected the timing of spawning and the subsequent growth of larvae.

We did not include an explicit representation of turbidity in the final version of our model. Turbidity affects spatial distributions (Feyrer et al. 2007; Nobriga et al. 2008) and larval growth (Baskerville-Bridges et al. 2004) of Delta Smelt. We initially included turbidity (estimated from extensive Secchi depth measurements) in the same way that we included salinity and temperature (Supplement A). Turbidity showed the expected decrease during the modeled time period, which is part of a longer-term downward trend (Kimmerer 2004; Wright and Schoellhamer 2004; Nobriga et al. 2008). However, we had no basis upon which to determine relationships between turbidity and growth rate or mortality rate, and thus we could have simulated a decline in the Delta Smelt population based solely on the lower turbidity in the later years. Because we predicted the decrease in Delta Smelt without turbidity (i.e., based on hydrodynamics, temperature, salinity, and zooplankton), a turbidity effect was not included.

In the companion paper (Rose et al. 2013), we further explore Delta Smelt dynamics using the individual-based model. We configure alternative baseline simulations and perform a simulation experiment to further refine our understanding of bad versus good years for Delta Smelt. We vary salinity, temperature, zooplankton, hydrodynamics, and eggs per entering age-1 individual between the best year (1998) and the worst year (2001) to systematically quantify the effects of each factor and their combined effects on λ. We then show that these results are robust to alternative baseline configurations.

ACKNOWLEDGMENTS

This project was funded by a grant from the CALFED Science Program (SCI-05-C106). We acknowledge the many people who discussed various aspects of the model and their willingness to discuss and provide information. Stephen Monismith helped with the PTM. Rachael Miller Neilan derived the Leslie model formulation. Erik Loboschefsky provided the DSM2 output files. Lindsay Sullivan shared data on Delta Smelt feeding, and Steve Slater provided diet data. We also had discussions during model development with Rick Sitts, Joan Lindberg, and Kevin Fleming; in addition, we held a workshop in Santa Cruz, where many people provided information and advice on the modeling in its early stages. The comments of two reviewers and the Associate Editor greatly improved the clarity of the paper.

REFERENCES

Baskerville-Bridges, B., J. C. Lindberg, and S. I. Doroshov. 2004. The effect of light intensity, alga concentration, and prey density on the feeding behavior of Delta Smelt larvae. Pages 219–227 *in* F. Feyrer, L. R. Brown, R. L. Brown, and J. J. Orsi, editors. Early life history of fishes in the San Francisco Estuary and watershed. American Fisheries Society, Symposium 39, Bethesda, Maryland.

Baxter, R., R. Breuer, L. Brown, L. Conrad, F. Feyrer, S. Fong, K. Gehrts, L. Grimaldo, B. Herbold, P. Hrodey, A. Mueller-Solger, T. Sommer, and K. Souza. 2010. 2010 pelagic organism decline work plan and synthesis of results. Interagency Ecological Program for the San Francisco Estuary, California Department of Water Resources, Sacramento.

Bennett, W. A. 2005. Critical assessment of the Delta Smelt population in the San Francisco Estuary, California. San Francisco Estuary and Watershed Science [online serial] 3(2):article 1.

Brown, L. R., W. Kimmerer, and R. Brown. 2009. Managing water to protect fish: a review of California's environmental water account, 2001–2005. Environmental Management 43:357–368.

Feyrer, F., M. L. Nobriga, and T. R. Sommer. 2007. Multidecadal trends for three declining fish species: habitat patterns and mechanisms in the San Francisco Estuary, California, USA. Canadian Journal of Fisheries and Aquatic Sciences 64:723–734.

Grimaldo, L. F., T. Sommer, N. Van Ark, G. Jones, E. Holland, P. B. Moyle, B. Herbold, and P. Smith. 2009. Factors affecting fish entrainment into massive water diversions in a tidal freshwater estuary: can fish losses be managed? North American Journal of Fisheries Management 29:1253–1270.

Grimm, V., U. Berger, F. Bastiansen, S. Eliassen, V. Ginot, J. Giske, J. Goss-Custard, T. Grand, S. K. Heinz, G. Huse, A. Huth, J. U. Jepsen, C. Jørgensen, W. M. Mooij, B. Müller, G. Pe'er, C. Piou, S. F. Railsback, A. M. Robbins, M. M. Robbins, E. Rossmanith, N. Rüger, E. Strand, S. Souissi, R. A. Stillman, R. Vabø, U. Visser, and D. L. DeAngelis. 2006. A standard protocol for describing individual-based and agent-based models. Ecological Modelling 198:115–126.

Grimm, V., E. Revilla, U. Berger, F. Jeltsch, W. M. Mooij, S. F. Railsback, H. H. Thulke, J. Weiner, T. Wiegand, and D. L. DeAngelis. 2005. Pattern-oriented modeling of agent-based complex systems: lessons from ecology. Science 310:987–991.

Gross, E. S., M. L. MacWilliams, C. D. Holleman, and T. A. Hervier. 2010. Particle tracking model testing and applications report. Report to the Interagency Ecological Program for the San Francisco Estuary, California Department of Water Resources, Sacramento.

Hanson, P. C., T. B. Johnson, D. E. Schindler, and J. F. Kitchell. 1997. Fish bioenergetics 3.0 software for Windows®. University of Wisconsin, Sea Grant Institute, Technical Report WISCU-T-97-001, Madison.

Hilborn, R. 2007. Reinterpreting the state of fisheries and their management. Ecosystems 10:1362–1369.

Hollibaugh, J. T., editor. 1996. San Francisco Bay: the ecosystem. American Association for the Advancement of Science, San Francisco.

Humston, R., J. S. Ault, M. Lutcavage, and D. B. Olson. 2000. Schooling and migration of large pelagic fishes relative to environmental cues. Fisheries Oceanography 9:136–146.

Humston, R., D. B. Olson, and J. S. Ault. 2004. Behavioral assumptions in models of fish movement and their influence on population dynamics. Transactions of the American Fisheries Society 133:1304–1328.

Kimmerer, W. J. 2004. Open water processes of the San Francisco Estuary: from physical forcing to biological responses. San Francisco Estuary and Watershed Science [online serial] 2(1):article 1.

Kimmerer, W. J. 2008. Losses of Sacramento River Chinook Salmon and Delta Smelt to entrainment in water diversions in the Sacramento–San Joaquin Delta. San Francisco Estuary and Watershed Science [online serial] 6(2):article 2.

Kimmerer, W. J. 2011. Modeling Delta Smelt losses at the south Delta export facilities. San Francisco Estuary and Watershed Science [online serial] 9(1):article 5.

Kimmerer, W. J., S. R. Avent, S. M. Bollens, F. Feyrer, L. F. Grimaldo, P. B. Moyle, M. Nobriga, and T. Visintainer. 2005. Variability in length–weight relationships used to estimate biomass of estuarine fish from survey data. Transactions of the American Fisheries Society 134:481–495.

Kimmerer, W. J., E. S. Gross, and M. L. MacWilliams. 2009. Is the response of estuarine nekton to freshwater flow in the San Francisco Estuary explained by variation in habitat volume? Estuaries and Coasts 32:375–389.

Kimmerer, W. J., and M. L. Nobriga. 2008. Investigating particle transport and fate in the Sacramento–San Joaquin Delta using a particle tracking model. San Francisco Estuary and Watershed Science [online serial] 6(1):article 4.

Lantry, B. F., and D. J. Stewart. 1993. Ecological energetics of Rainbow Smelt in the Laurentian Great Lakes: an interlake comparison. Transactions of the American Fisheries Society 122:951–976.

Lott, J. 1998. Feeding habits of juvenile and adult Delta Smelt from the Sacramento–San Joaquin River Estuary. Interagency Ecological Program Newsletter 11(1):14–19.

Lund, J. R., E. Hanak, W. E. Fleenor, W. A. Bennett, R. E. Howitt, J. F. Mount, and P. B. Moyle. 2010. Comparing futures for the Sacramento–San Joaquin Delta. University of California Press, Berkeley.

Mac Nally, R., J. R. Thomson, W. J. Kimmerer, F. Feyrer, K. B. Newman, A. Sih, W. A. Bennett, L. Brown, E. Fleishman, S. D. Culberson, and G. Castillo. 2010. Analysis of pelagic species decline in the upper San Francisco Estuary using multivariate autoregressive modeling (MAR). Ecological Applications 20:1417–1430.

Maunder, M. N., and R. B. Deriso. 2011. A state–space multistage life cycle model to evaluate population impacts in the presence of density dependence: illustrated with application to Delta Smelt (*Hypomesus transpacificus*). Canadian Journal of Fisheries and Aquatic Sciences 68:1285–1306.

McCann, K., and B. Shuter. 1997. Bioenergetics of life history strategies and the comparative allometry of reproduction. Canadian Journal of Fisheries and Aquatic Sciences 54:1289–1298.

McGranahan, G., D. Balk, and B. Anderson. 2007. The rising tide: assessing the risks of climate change and human settlements in low elevation coastal zones. Environment and Urbanization 19:17–37.

Miller, A. 2002. Particle tracking model verification and calibration. Pages 2.1–2.25 *in* M. Mierzwa, editor. Methodology for flow and salinity estimates in the Sacramento–San Joaquin Delta and Suisun marsh. California Department of Water Resources, Office of State Water Project Planning, 23rd Annual Progress Report, Sacramento. Available: modeling.water.ca.gov/delta/reports/annrpt/2002/2002Ch2.pdf. (November 2012).

Miller, W. J. 2011. Revisiting assumptions that underlie estimates of proportional entrainment of Delta Smelt by state and federal water diversions from the Sacramento–San Joaquin Delta. San Francisco Estuary and Watershed Science [online serial] 9(1):article 4.

Miller, W. J., B. F. J. Manly, D. D. Murphy, D. Fullerton, and R. R. Ramey. 2012. An investigation of factors affecting the decline of Delta Smelt (*Hypomesus transpacificus*) in the Sacramento–San Joaquin Estuary. Reviews in Fisheries Science 20:1–19.

Moyle, P. B. 2002. Inland fishes of California, revised and expanded. University of California Press, Berkeley.

Moyle, P. B., B. Herbold, D. E. Stevens, and L. W. Miller. 1992. Life history and status of Delta Smelt in the Sacramento–San Joaquin Estuary, California. Transactions of the American Fisheries Society 121:67–77.

Myers, R. A., and B. Worm. 2003. Rapid worldwide depletion of predatory fish communities. Nature 423:280–283.

Newman, K. B. 2008. Sample design-based methodology for estimating Delta Smelt abundance. San Francisco Estuary and Watershed Science [online serial] 6(3):article 3.

Ney, J. J. 1993. Bioenergetics modeling today: growing pains on the cutting edge. Transactions of the American Fisheries Society 122:736–748.

Nichols, F. H., J. E. Cloern, S. N. Luoma, and D. H. Peterson. 1986. The modification of an estuary. Science 231:567–573.

Nichols, F. H., J. K. Thompson, and L. E. Schemel. 1990. Remarkable invasion of San Francisco Bay (California, USA) by the Asian clam *Potamocorbula amurensis:* II. displacement of a former community. Marine Ecology Progress Series 66:95–101.

Nobriga, M. L. 2002. Larval Delta Smelt diet composition and feeding incidence: environmental and ontogenetic influences. California Fish and Game 88:149–164.

Nobriga, M. L., T. R. Sommer, F. Feyrer, and K. Fleming. 2008. Long-term trends in summertime habitat suitability for Delta Smelt (*Hypomesus transpacificus*). San Francisco Estuary and Watershed Science [online serial] 6(1):article 1.

NRC (National Research Council). 2010. A scientific assessment of alternatives for reducing water management effects on threatened and endangered fishes in California's Bay–Delta. National Academies Press, Washington, D.C.

NRC (National Research Council). 2012. Sustainable water and environmental management in the California Bay–Delta. National Academies Press, Washington, D.C.

Rose, K. A. 2000. Why are quantitative relationships between environmental quality and fish populations so elusive? Ecological Applications 10:367–385.

Rose, K. A., A. T. Adamack, C. A. Murphy, S. E. Sable, S. E. Kolesar, J. K. Craig, D. L. Breitburg, P. Thomas, M. H. Brouwer, C. F. Cerco, and S. Diamond. 2009. Does hypoxia have population-level effects on coastal fish? musings from the virtual world. Journal of Experimental Marine Biology and Ecology 381(Supplement):188–203.

Rose, K. A., W. J. Kimmerer, K. P. Edwards, and W. A. Bennett. 2013. Individual-based modeling of Delta Smelt population dynamics in the upper San Francisco Estuary: II. Alternative baselines and good versus bad years. Transactions of the American Fisheries Society 142:1260–1272.

Scheffer, M., J. M. Baveco, D. L. DeAngelis, K. A. Rose, and E. H. van Nes. 1995. Super-individuals: a simple solution for modelling large populations on an individual basis. Ecological Modelling 80:161–170.

Sommer, T., C. Armor, R. Baxter, R. Breuer, L. Brown, M. Chotkowski, S. Culberson, F. Feyrer, M. Gingras, B. Herbold, W. Kimmerer, A. Mueller-Solger, M. Nobriga, and K. Souza. 2007. The collapse of pelagic fishes in the upper San Francisco Estuary. Fisheries 32:270–277.

Sommer, T., F. Mejia, M. Nobriga, F. Feyrer, and L. Grimaldo. 2011. The spawning migration of Delta Smelt in the upper San Francisco Estuary. San Francisco Estuary and Watershed Science [online serial] 9(2):article 2.

Stow, C. A., J. Jolliff, D. J. McGillicuddy Jr., S. C. Doney, J. I. Allen, M. A. M. Friedrichs, K. A. Rose, and P. Wallhead. 2009. Skill assessment for coupled biological/physical models of marine systems. Journal of Marine Systems 76:4–15.

Thomson, J. R., W. J. Kimmerer, L. R. Brown, K. B. Newman, R. Mac Nally, W. A. Bennett, F. Feyrer, and E. Fleishman. 2010. Bayesian change point analysis of abundance trends for pelagic fishes in the upper San Francisco Estuary. Ecological Applications 20:1431–1448.

Tyler, J. A., and K. A. Rose. 1994. Individual variability and spatial heterogeneity in fish population models. Reviews in Fish Biology and Fisheries 4:91–123.

Vörösmarty, C. J., P. Green, J. Salisbury, and R. B. Lammers. 2000. Global water resources: vulnerability from climate change and population growth. Science 289:284–288.

Wilbur, R. J. 2000. Validation of dispersion using the particle tracking model in the Sacramento–San Joaquin Delta. Master's thesis. University of California, Davis. Available in condensed form: modeling.water.ca.gov/delta/reports/annrpt/2001/2001Ch4.pdf. (November 2012).

Wilensky, U., and W. Rand. 2007. Making models match: replicating an agent-based model. Journal of Artificial Societies and Social Simulation [online serial] 10(4):2. Available: jasss.soc.surrey.ac.uk/10/4/2.html. (November 2012).

Winder, M., and A. D. Jassby. 2011. Shifts in zooplankton community structure: implications for food web processes in the upper San Francisco Estuary. Estuaries and Coasts 34:675–690.

Winemiller, K. O., and K. A. Rose. 1992. Patterns of life-history diversification in North American fishes: implications for population regulation. Canadian Journal of Fisheries and Aquatic Sciences 49:2196–2218.

Worm, B., R. Hilborn, J. K. Baum, T. A. Branch, J. S. Collie, C. Costello, M. J. Fogarty, E. A. Fulton, J. A. Hutchings, S. Jennings, O. P. Jensen, H. K. Lotze, P. M. Mace, T. R. McClanahan, C. Minto, S. R. Palumbi, A. M. Parma, D. Ricard, A. A. Rosenberg, R. Watson, and D. Zeller. 2009. Rebuilding global fisheries. Science 325:578–585.

Wright, S. A., and D. H. Schoellhamer. 2004. Trends in the sediment yield of the Sacramento River, California, 1957–2001. San Francisco Estuary and Watershed Science [online serial] 2(2):article 2.